Ecological Modelling 359 (2017) 415–433

Contents lists available at ScienceDirect

Ecological Modelling

journal homepage: www.elsevier.com/locate/ecolmodel

Modelling the plankton groups of the deep, peri-alpine Lake Bourget

Onur Kerimoglu[a,b,*], Stéphan Jacquet[b], Brigitte Vinçon-Leite[c], Bruno J. Lemaire[c], Frédéric Rimet[b], Frédéric Soulignac[c], Dominique Trévisan[b], Orlane Anneville[b]

[a] Helmholtz-Zentrum Geesthacht, Max-Planck-str. 1, 21502 Geesthacht, Germany
[b] Hydrobiological Station, INRA, UMR CARRTEL, BP 511, Thonon Cedex, France
[c] Laboratoire Eau Environnement Systeèmes Urbains, Ecole des Ponts ParisTech, UPEC, AgroParisTech, UPE, Marne-la-Vallée, France

ARTICLE INFO

Article history:
Received 15 August 2016
Received in revised form 6 June 2017
Accepted 7 June 2017

Keywords:
Coupled physical-biological model
Re-oligotrophication
Cyanobacteria
Mixotrophy
Allometry
Priority effect
Bistability

ABSTRACT

Predicting phytoplankton succession and variability in natural systems remains to be a grand challenge in aquatic ecosystems research. In this study, we identified six major plankton groups in Lake Bourget (France), based on cell size, taxonomic properties, food-web interactions and occurrence patterns: cyanobacterium *Planktothrix rubescens*, small and large phytoplankton, mixotrophs, herbivorous and carnivorous zooplankton. We then developed a deterministic dynamic model that describes the dynamics of these groups in terms of carbon and phosphorus fluxes, as well as of particulate organic phosphorus and dissolved inorganic phosphorus. The modular and generic model scheme, implemented as a set of modules under Framework for Aquatic Biogeochemical Models (FABM) enables run-time coupling of the plankton module an arbitrary number of times, each time with a prescribed position across the autotrophy/heterotrophy continuum. Parameters of the plankton groups were mainly determined conjointly by the taxonomic and allometric relationships, based on the species composition and average cellular volume of each group. The biogeochemical model was coupled to the one-dimensional General Ocean Turbulence Model (GOTM) and forced with local meteorological conditions. The coupled model system shows very high skill in predicting the spatiotemporal distributions of water temperature and dissolved inorganic phosphorus for five simulated years within the period 2004 to 2010, and intermediate skill in predicting the plankton succession. We performed a scenario analysis to gain insight into the factors driving the sudden disappearance of *P. rubescens* in 2010. Our results provide evidence for the hypothesis that the abundance of this species before the onset of stratification is critical for its success later in the growing season, pointing thereby to a priority effect.

1. Introduction

Mechanistic ecosystem models are not only ideal media for synthesizing data and theory and thereby improving our understanding of the functioning of ecosystems, but they are also useful tools for supporting decision-making processes. Implementation of ecosystem models in aquatic systems has been increasingly appearing in the form of coupled hydrodynamic-biogeochemical models, reflecting the increasing recognition that biogeochemistry is often strongly driven by hydrodynamics, as well as the advances in computing power (Robson, 2014).

While coupled hydrodynamic-biogeochemical models can often provide reliable estimates of physical parameters such as temperature and salinity, prediction of chemical and biological parameters, and especially occurrence of certain plankton species or functional groups are more difficult to predict (Shimoda and Arhonditsis, 2016). Problems start there already at the very preliminary stage of conceptual model building: what constitutes a functional group? From a global perspective, Hood et al. (2006) defined a functional group as an entity that plays a particular role in a certain biogeochemical pathway, such as nitrogen fixation or silification. However, shifts in the community structure under focus might be driven by competition for the shared resources or trophic interactions, intensity of which may change across seasonal to interdecadal scales, e.g., with thermal stratification dynamics and changes in nutrient loading (Sommer et al., 2012; Kerimoglu et al., 2013). In such cases, traits relating to growth rate, grazer defense, resource utilization, temperature response and motility (Litchman et al., 2010) should (also) be considered for identifying the functional groups, for which, ample examples indeed exist (Jöhnk et al., 2008; Mieleitner and Reichert, 2008; Carraro et al., 2012).

* Corresponding author.
E-mail address: kerimoglu.o@gmail.com (O. Kerimoglu).

http://dx.doi.org/10.1016/j.ecolmodel.2017.06.005
0304-3800/

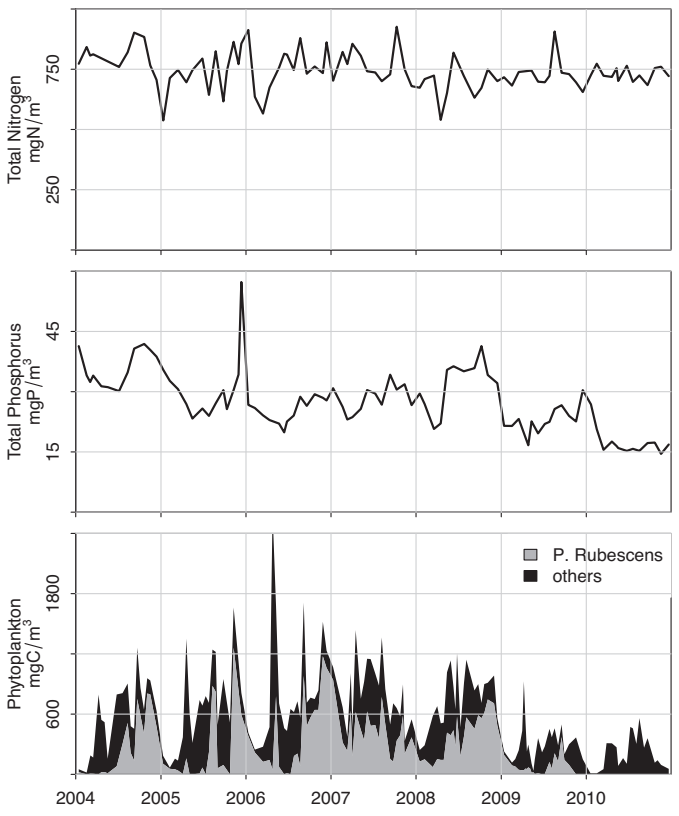

Fig. 1. Observed concentrations of total phosphorus and total nitrogen (0–140 m average), and total phytoplankton and contribution by *P. rubescens* in Lake Bourget (0–20 m average) for the period 2004–2010.

The system under investigation here, Lake Bourget, France, has been recovering from eutrophication since the 1980s (Vinçon-Leite et al., 1995; Jacquet et al., 2014a). Starting from 1996, the toxic cyanobacterium, *Planktothrix rubescens* became a dominant species in the lake (Vinçon-Leite et al., 2002; Jacquet et al., 2005, see also Fig. 1). *P. rubescens* is a wide-spread cyanobacterial species especially prevalent in peri-alpine lakes (e.g., Ernst et al., 2009; Salmaso et al., 2012; Dokulil and Teubner, 2012; Posch et al., 2012), but also observed elsewhere (e.g., Konopka, 1982; Halstvedt et al., 2007; Naselli-Flores et al., 2007; Padisák et al., 2010). Being a potentially microcystin producing species (Briand et al., 2005), its occurrence in lakes and reservoirs has been of major concern for livestock and human health (Naselli-Flores et al., 2007; Ernst et al., 2009). In 2010, *P. rubescens* suddenly disappeared (Jacquet et al., 2014b) from Lake Bourget, whereas the mixotrophic and small phytoplankton species became relatively more abundant, latter being typical for oligotrophic systems (Anneville et al., 2004; Chen and Liu, 2010; Mitra et al., 2014). Accordingly, mixotrophy and traits associated with cell size should be taken into account for understanding the mechanisms driving the changes in phytoplankton community composition, and in particular, the disappearance of *P. rubescens* in Lake Bourget.

Since long, phytoplankton cell size has been recognized to be an important aspect in determining the ecophysiology of phytoplankton (e.g., Finkel et al., 2010; Litchman et al., 2010, and references therein), and cell size has been increasingly used as a 'master trait' (Litchman et al., 2010) in theoretical modelling studies (e.g., Grover, 1991; Armstrong, 1994; Litchman et al., 2009; Kerimoglu et al., 2012, submitted), although the integration of size concept in realistic ecosystem models attempting to reproduce mesocosm or field observations at relevant ecological time scales has been gaining momentum only recently (but see, e.g., Ward et al., 2012; Wirtz, 2013; Terseleer et al., 2014). Following many decades of dichotomous classification of planktonic organisms as 'autotrophs' and 'heterotrophs' (Flynn et al., 2012), importance of mixotrophy in ecosystem functioning has been increasingly recognized (Mitra et al., 2014, and references therein). Mixotrophy has been addressed mainly by theoretical work so far (e.g., Thingstad et al., 1997; Flynn and Mitra, 2009; Crane and Grover, 2010; Berge et al., 2017). The recent work of Ward and Follows (2016) constitutes the first example where mixotrophy is resolved in a global ocean model.

Environmental control of the occurrence of *P. rubescens* blooms is still under debate. Analysis of the long-term changes in individual lakes and inter-comparison between lakes suggest that phosphorus (and nitrogen, see Posch et al., 2012) availability is the primary determinant (Dokulil and Teubner, 2012; Jacquet et al., 2014b; Anneville et al., 2015). *P. rubescens* is characterized by their slow growth rates (Bright and Walsby, 2000) and tolerance to low light conditions (Walsby and Schanz, 2002). As a result of the latter, it often develops thin and intense layers within the metalimnion during the growing season (e.g., Jacquet et al., 2014b), where they are the first to harvest the nutrients leaking from the nutrient-rich layers beneath the thermocline. On the other hand, occurrence of *P. rubescens* displays extreme interannual variability in deep lakes, which is suggested to be driven by meteorological conditions (Vinçon-Leite et al., 2002; Salmaso, 2010; Jacquet et al., 2014b; Anneville et al., 2015): after warm winters, *P. rubescens* have been observed to be at relatively high abundances, which is usually followed by their sustained dominance throughout the growing season (Salmaso, 2010; Posch et al., 2012).

In this study, we had the following objectives: (1) developing a plankton model that resolves mixotrophy and relies on allometric relationships for the parameterization of plankton groups; (2) implementing the plankton model in a 1-D coupled hydrodynamical-biogeochemical modeling framework for the simulation of the surface layer dynamics of Lake Bourget; (3) quantifying the performance of the model with respect to both the bulk characteristics of the system and plankton groups; (4) gaining insight into the reasons for the relative importance of low phosphorus concentrations and low starting inoculum at the beginning of the growth season for the disappearance of *P. rubescens* in Lake Bourget.

2. Study site and data

The study site is Lake Bourget, a peri-alpine (45°44′N, 5°52′E, 231 m altitude) lake with a maximum depth of 145 m and a surface area of approximately 45 km^2. It has a north-south aligned, elongated basin with a length of 18 km and a maximal width of 3 km at the surface. Within the study period (2004–2010), average total phosphorus and nitrogen concentration ranged between approximately 15–45 mg/m^3 and 550–800 mg/m^3, respectively (Fig. 1), classifying it as a mesotrophic system. Further details about the lake can be found in Vinçon-Leite et al. (1995) and Jacquet et al. (2014b).

Meteorological data required to force the hydrodynamical model (see Section 4.3) were taken from the Météo-France station at Vouglans, located at the southern tip of Lake Bourget. In-situ data used in this study were sampled at the deepest location of Lake Bourget. Sampling was performed usually biweekly during the growth season and monthly during winter. Water temperature was measured at high vertical resolution with a conductivity-temperature-depth probe, and interpolated on a regular grid of 1-m intervals. Nutrient data were collected at several irregular depths (2, 10, 15, 20, 30, 50, 80, 110, 130, 140 m), and interpolated also to a regular 1-m grid. For the phytoplankton species counts, an

Table 1
Properties of algal/mixotroph groups, averaged for the period 2004–2010. % Contr.: percentage contribution to the total biovolume of phytoplankton and mixotrophs; V: biovolume-weighted average volume of the group.

Class	% Contr.	V [μm^3]
Small	22.9	236.9
Large	15.5	13717.1
P. rubescens	40.1	84.8
Mixotrophs	21.3	12978.8

integrating sampler was used for the 2.5 times Secchi depth in 2005 (typically between 10 and 20 m) and for the top 20 m after 2005. For the zooplankton species counts, depth-averaged samples were taken with 0–50 m hauls. Further details on the regular sampling programme of Lake Bourget can be found in Jacquet et al. (2014a). Conversion of the phytoplankton species counts to carbon biomass was based on biovolume of each species (Druart and Rimet, 2008), and assuming 0.2 pgC/μm^3. Zooplankton counts were first converted into wet weight, 10% of which was assumed to be dry weight (Dumont et al., 1975), from which the carbon biomasses were calculated assuming that carbon constitutes 48% of dry weight (Andersen and Hessen, 1991).

3. Identification of functional groups

3.1. Algae and mixotrophs

We defined 3 functional algal groups and a mixotroph group. The first group consists of only *P. rubescens* (abbreviated A_{PR} hereafter), reflecting the unique eco-physiological properties of this species, and its abundance in Lake Bourget (Table 1). Second is the 'small algae' group (A_S), consisting of all species with cell volume up to 10^3 μm^3, and not being mixotrophs (see below), comprising cyanobacteria (except *P. rubescens*), diatoms, chlorophyta and chrysophyta (Table A2). Third is the 'large algae' group (A_L), those with cell volume larger than 10^3 μm^3, and not being mixotrophs. Finally, the 'mixotroph' group (M), consists of species with cell volume $\geq 10^2$ μm^3 and belonging to Chrysophyta, Dinophyta and Cryptophyta.

In Table 1, 2004–2010 average biovolume fraction and biovolume-weighted cell volume of each algal and mixotroph group are provided.

3.2. Zooplankton

We considered two zooplankton groups: herbivores (Z_H), dominated by *Daphnia* sp., *Diaphanosoma* and *Eudiaptamus* species (Table A1) and are considered to feed on phytoplankton and detritus (see the model description, Section 4.1); and carnivores (Z_C), dominated by cyclopoid copepodits of stages C5 and C6, and are considered to feed on herbivorous zooplankton, mixotrophs and large algae.

4. The model

As a spatially explicit model, temporal and spatial changes in the volumetric concentration of a biological state variable, c_i with units mmol/m^3, are described by a system of partial differential equations of the generic form:

$$\frac{\partial c_i}{\partial t} + \frac{\partial}{\partial z}\left(\omega_i(t,z)c_i(t,z) - K_z(t,z)\frac{\partial c_i(t,z)}{\partial z}\right) = s(c_i(t,z)) \quad (1)$$

where w_i the vertical motion, K_z the eddy diffusivity and $s(c_i)$ the net source term (production-destruction) resulting from biological interactions.

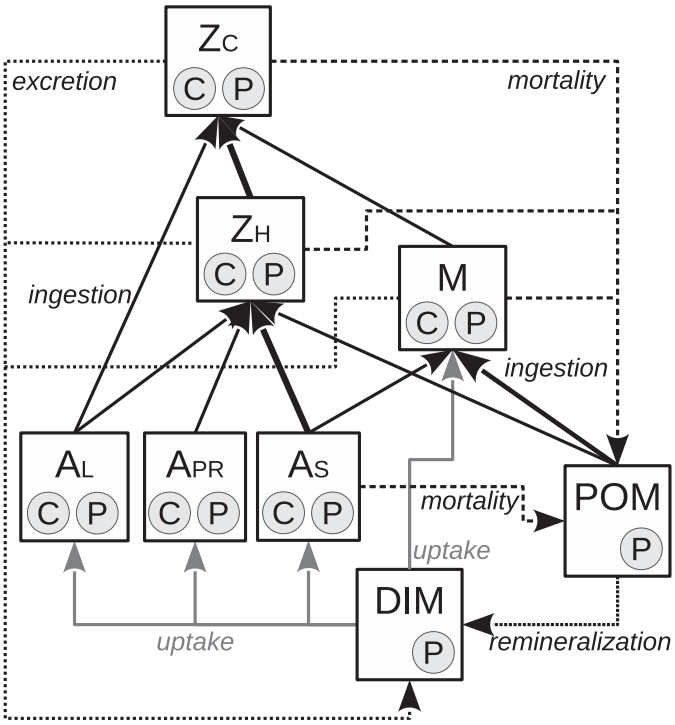

Fig. 2. Model structure. DIM: dissolved inorganic matter (here phosphorus only, so referred to as DIP hereafter), POM: particulate organic matter (here phosphorus only, so referred to as POP hereafter), A_{PR}: *P. rubescens*, A_l: large algae, A_s: small algae, M: mixotrophs, Z_H: herbivorous zooplankton, Z_C: carnivorous zooplankton. Thick arrows indicate strong feeding preference. C and P in circles indicate carbon and phosphorus.

Structure of the biological model is depicted in Fig. 2. As phosphorus is recognized to be the primary determinant of phytoplankton dynamics in Lake Bourget (Jacquet et al., 2005, 2014b), only phosphorus limitation was considered in this study. The model describes the interactions and phosphorus fluxes in the lower trophic food-web, by resolving particulate and dissolved inorganic phosphorus pools and 6 plankton groups (Section 3), in terms of carbon and phosphorus content. Detailed description of the biological model, i.e., the source terms in Eq. (1) are provided in Section 4.1.

The biological model is coupled to the 1-D water column model General Ocean Turbulence Model (GOTM) via the Framework for Aquatic Biogeochemical Models (FABM), providing the ambient water temperature and photosynthetically active radiance (see Section 4.1), as well as performing the numerical integration, including the transport terms in Eq. (1). Further information about the physical model and coupling are provided in Sections 4.3–4.4.

4.1. Biological model

In this study, instead of describing autotrophs, heterotrophs and mixotrophs separately, we describe a generic plankton unit that can be anything between a pure autotroph or a pure heterotroph, inspired by the 'mixotroph species' in Crane and Grover (2010). A central parameter in this unified representation is the fraction of photosynthethic autotrophy, ζ, set to $\zeta = 1.0$ for 3 autotroph groups (X_i={A_{PR}, A_L, A_S}), $\zeta = 0.5$ for the mixotrophs (X_i={M}) and $\zeta = 0.0$ for the zooplankton (X_i={Z_H, Z_C}) (Table 3, see section 3 for the identification of functional groups).

The complete set of equations describing the dynamics of carbon (X^C) and phosphorus (X^P) bound to plankton, for X_i={A_{PR}, A_L,

Table 2
Definition and units of state variables, processes and intermediate quantities.

Symbol	Unit	Definition
X^C	mmolC m^{-3}	C bound to plankton
X^P	mmolP m^{-3}	P bound to plankton
POP	mmolP m^{-3}	Particulate organic phosphorus
DIP	mmolP m^{-3}	Dissolved inorganic phosphorus
Q	molP molC^{-1}	Phosphorus quota
$\mu^{C(P)}$	d^{-1}	C (P) limited growth rate
P	d^{-1}	Photosynthesis rate
G_{jk}	d^{-1}	Ingestion rate of prey k by predator j
U	molP molC^{-1} d^{-1}	Nutrient uptake rate
L	d^{-1}	Mortality rate

A_S, M, Z_H, Z_C}, particulate organic phosphorus (POP) and dissolved inorganic phosphorus (DIP) is given in Eqs. (2a)–(2d).

$$s(X_i^C) = \min(\mu^P, \mu^C)X_i^C - (e_i + L_i)X_i^C - \sum_j (1-\zeta_j)(G_{j,k=i}X_j^C) \quad (2a)$$

$$s(X_i^P) = \epsilon_i^P \left(\zeta_i U_i + (1-\zeta_i)\sum_k G_{j=i,k}Q_k \right) X_i^C - (e_i + L_i)X_i^P - \sum_j (1-\zeta_j)G_{j,k=i}Q_k X_i^C \quad (2b)$$

$$s(POP) = \sum_i L_i X_i^P - \sum_j (1-\zeta_j)G_{j,k=POP}X_j^C - rPOP \quad (2c)$$

$$s(DIP) = \sum_i (1-\zeta_i)(1-\epsilon_i^P)X_i^C \sum_k G_{j=i,k}Q_k - \sum_i \epsilon_i^P \zeta_i U_i X_i^C + \sum_i e_i X_i^P + rPOP \quad (2d)$$

Definition and units of state variables, major processes, intermediate quantities and parameters are provided in Tables 2–5. Additional terms are introduced upon their appearance when necessary. In Eqs. (2a–2d) and below, index i stands for each of the 6 plankton groups considered here (Fig. 2), and indices j and k stand respectively for the predator and prey items.

In Eq. (2a), the first term describes biomass gain, as a minimum function of carbon and phosphorus limited growth. Nutrient limited growth, μ^P is represented with the Droop equation (Droop, 1968) for autotrophs and mixotrophs, i.e., for the non-homeostatic case:

$$\text{if } Q_{\min} < Q_{\max}: \quad \mu^P = \mu_\infty f_Q = \mu_\infty \left(1 - \frac{Q_{\min}}{Q}\right) \quad (3)$$

where f_Q describes quota-dependent nutrient limitation of biomass growth. For pure heterotrophs ($\zeta = 0$, Table 3), which are assumed to be homeostatic ($Q_{max} = Q_{min}$, Table 3), nutrient limitation is assumed to be absent, i.e. only the carbon limited growth is taken into account ($\mu^P = \infty$).

Carbon limited growth rate is calculated as the sum of specific carbon fixation rate through photosynthesis and carbon assimilation rate through heterotrophy:

$$\mu^C = \zeta_i P_i + (1-\zeta_i)\epsilon_i^C \sum_k G_{j=i,k} \quad (4)$$

Photosynthetic carbon fixation rate is calculated as a function employed by Schwaderer et al. (2011) that accounts for inhibition at high irradiances:

$$P = \mu_{\max} f_I = \frac{\mu_{\max} I_{PAR}}{I^2 \frac{\mu_{\max}}{\alpha I_{opt}^2} + I(1 - 2\frac{\mu_{\max}}{\alpha I_{opt}}) + \frac{\mu_{\max}}{\alpha}} \quad (5)$$

where $\mu_{max} = \mu_P(Q_{max})$ (Eq. (3)), f_I describe light limitation and I_{PAR} stands for photosynthetically active radiation.

Heterotrophic carbon assimilation rate in Eq. (4) is given by the product of total ingestion rate and carbon assimilation efficiency, ϵ^C (Table 3 and section 4.2.2). Ingestion rate of the each prey item is described by:

$$G_{j=i,k} = G_{i,\max} \frac{p_{j=i,k} X_k^C}{K_{G,i} + \sum_k p_{j=i,k} X_k^C} \quad (6)$$

where $p_{j,k}$ is the preference of zooplankton j for the food item k (Table 5), and $X^C_{k=POP}$=POC was calculated as $POC = POP/Q_{POM}$, assuming Redfield ratio for Q_{POM} (Table 4). Copepods are known to switch between filtering and raptorial feeding behaviors based on the food availability (Kiørboe, 2011), which is here accounted by adjusting the feeding preferences of Z_C based on relative abundance, as in (Fasham et al., 1990):

$$p'_{j,k} = \frac{p_{j,k} X_k}{\sum_k p_{j,k} X_k} \quad (7)$$

where $p'_{j,k}$ replaces $p_{j,k}$ in Eq. (6).

Analogous to Eq. (2a), the first term in Eq. (2b) describes the cumulative phosphorus binding rate through uptake of dissolved nutrients and nutrient assimilation rate of the ingested food. Uptake rate of dissolved nutrients is represented according to the Michaelis-Menten kinetics:

$$U = U_{\max} f_N = U_{\max} \frac{DIP}{DIP + K_U} \quad (8)$$

where f_N describes nutrient limitation of nutrient uptake rate. Regulation of nutrient assimilation differs between homeostatic and non-homeostatic organisms in our model: In the non-homeostatic case, (i.e., $Q_{min} < Q_{max}$) as in phytoplankton and mixotrophs, nutrient uptake rate is adjusted by ϵ^P, as a linear function of nutrient quota as described in Eq. (9):

$$\text{if } Q_{\min} < Q_{\max}: \quad \epsilon^P = \frac{Q_{\max} - Q}{Q_{\max} - Q_{\min}} \quad (9)$$

which stems from the Droop model describing down regulation of nutrient uptake (Morel, 1987,, with the lower boundary of U_{max} being 0), and generalized by Crane and Grover (2010) to apply also for assimilation of ingested nutrients (Eq. (2b)). The final, quota-adjusted nutrient uptake rate appears as a sink term in Eq. (2d), summed across all plankton (multiplied by their autotrophic fractions).

In the case of homeostatic regulation of carbon and phosphorus assimilation (i.e., $Q_{min} = Q_{max}$), the guiding assumption is that stoichiometry of elemental gains should be equal to the stoichiometry of the organism (Eq. (10)). There are then two possibilities: If the carbon gain would exceed phosphorus gain with the default assimilation efficiencies, carbon assimilation efficiency is re-adjusted (Eq. (11)). This implies decreasing specific growth rate with decreasing Q_k (of prey) when $Q_k < Q_j$ for a fixed prey concentration, which is in line with observations (Hessen et al., 2013). On the other hand, if phosphorus gain exceeds carbon gain, P-assimilation efficiency is re-adjusted (Eq. (12)), similar to Grover (2002).

$$\text{if } Q_{\min} = Q_{\max} = Q: \quad \frac{\epsilon_i^P \sum_k G_{j=i,k} Q_k}{\epsilon_i^C \sum_k G_{j=i,k}} = Q_i \quad (10)$$

$$\text{if } Q_i \epsilon_i^C \sum_k G_{j=i,k} > \epsilon_i^P \sum_k G_{j=i,k} Q_k: \quad \epsilon_i^C = \frac{\epsilon_i^P \sum_k G_{j=i,k} Q_k}{Q_i \sum_k G_{j=i,k}} \quad (11)$$

Table 3
Model parameters specific to plankton groups. Horizontal lines separate the parameters relevant for all plankton, only autotrophs and only heterotrophs.

Symbol	Unit	Definition	A_S	A_L	A_{PR}	M	Z_H	Z_C
ζ	–	Fraction of autotrophy	1	1	1	0.5	0	0
w	m d^{-1}	Sinking velocity	0	-0.1	0	0	0	0
l^q	d^{-1} m^3 $mmolC^{-3}$	Quadratic mort. rate	0.001	0.001	0.001	0.01	0.02	0.04
l	d^{-1}	Linear mortality rate	0.02	0.02	0.02	0.02	0.02	0.02
e	d^{-1}	Excretion rate	0	0	0	0.01	0.02	0.02
Q_{max}	molP $molC^{-1}$	Upper bound of P quota	0.0145	0.04	0.0145	0.0082	0.0117	0.005
Q_{min}	molP $molC^{-1}$	Subsistence quota	0.00145	0.004	0.00145	0.0045	0.0117	0.005
μ_∞	d^{-1}	μ at $Q\rightarrow\infty$	1.2	1	0.39	1.22	–	–
α	d^{-1} W^{-1} m^2	Slope of the P-I curve	0.1	0.2	0.4	0.05	–	–
I_{opt}	W m^{-2}	Optimal I	40	30	10	40	–	–
K_U	mmolP m^{-3}	Half sat. *DIP* for U	0.2	0.4	1	1	–	–
U_{max}	molP $molC^{-1}$ d^{-1}	Max. uptake rate	0.139	0.038	0.146	0.065	–	–
G_{max}	d^{-1}	Max. grazing rate	–	–	–	2.79	1.66	1.15
K_G	mmolC m^{-3}	Half. sat. X^C for G	–	–	–	20	20	20
ϵ^C	–	Carbon assim. eff.	–	–	–	0.42	0.3	0.3

Table 4
Model parameters that are not specific to plankton groups.

Symbol	Unit	Definition	Value
r	d^{-1}	Remineralization rate	0.15
$k_{c,phy}$	m^2 $mmolC^{-1}$	Specific light ext. coef.	0.03
$k_{c,det}$	m^2 $mmolC^{-1}$	Specific light ext. coef.	0.02
w_{POP}	m d^{-1}	Sinking rate	−1.0
Q_{POM}	molP $molC^{-1}$	P:C ratio of POM	1/116
T_{ref}	°C	Reference temperature	20
$Q10_B$	–	Q10 for bacteria	1.5
$Q10_A$	-	Q10 for autotrophs	1.5
$Q10_H$	-	Q10 for heterotrophs	2

Table 5
Model parameters: grazing preferences $p_{j,k}$ of predator j (rows) for prey k (columns). – stands for $p_{j,k}=0$. $'$ for Z_C indicates that preferences are dynamically adjusted (see Eq. (7)).

	POM	A_S	A_{PR}	A_L	M	Z_H
M	0.6	0.4	–	–	–	–
Z_H	0.2	0.5	0.1	0.2	–	–
Z_C'	–	–	–	0.2	0.2	0.6

$$\text{else}: \quad \epsilon_i^P = \frac{Q_i \epsilon_i^C \sum_k G_{j=i,k}}{\sum_k G_{j=i,k} Q_k} \tag{12}$$

In both homeostatic/non-homeostatic cases, the unassimilated portion of the ingested or taken-up phosphorus ($(1-\epsilon_i^P)\sum_k G_{j=i,k}Q_k$) is added back to the DIP pool (Eq. (2d)).

Last two terms in Eqs. (2a–2b) correspond to excretion, mortality and losses caused by predation by other plankton groups. Excretion is assumed to be associated with heterotrophy (0 for purely autotroph plankton), occurs at a fixed specific rate (Table 3) and is recycled back as *DIP* (Eq. (2d)). Planktonic losses due to mortality is recycled as *POP*, and is the sum of a constant rate and a specific rate that linearly scales with X^C, accounting for losses to parasites and unresolved higher predators (Steele and Henderson, 1992):

$$L_i = l_i + l_i^q X_i^C \tag{13}$$

Gas vesicles of *P. rubescens* are known to collapse at high pressures (70–90 m in the strains found in Lake Zurich Walsby et al., 1998). In reality, this only affects their buoyancy, and consecutively leads to an increased sedimentation of *P. rubescens*, but as we do not explicitly account for buoyancy in this study, we mimic this effect by parameterizing the mortality rate of A_{PR} as a sigmoidal function of depth, that has the infliction point at $z=40$ m, converging to $l'_{i=PR}$ (=0.02 d^{-1}, as all other plankton, see Table 3) at the surface, and $5{*}l'_{i=PR}$ (=0.1 d^{-1}) towards 80 m:

$$l_{i=PR} = l'_{i=PR}\left(1 + 4\frac{1}{1+e^{0.1(40-z)}}\right) \tag{14}$$

Ingestion appears as a sink term for *POP* (Eq. (2c)), which is assumed to be a food source for mixotrophs (Table 5). Last terms in (2c)-(2d) describe remineralization of organic phosphorus O^P into dissolved inorganic form DIP at a fixed rate r.

Finally, temperature dependence of all reaction rates was included in the model through the Q10 rule:

$$rate(T) = rate(T = T_{ref}) f_T \tag{15}$$

$$f_T(Q10) = Q10^{(T-T_{ref})/T_{ref}} \tag{16}$$

where T is the ambient water temperature in ° C, which is provided by the physical model. For remineralization (r), Eq. (15) directly applies, where f_T in Eq. (16) is computed with the $Q10_B$ for bacteria (Table 4), whereas for plankton, f_T in Eq. (15) is replaced by a response function f'_T obtained by weighing the autotrophic and heterotrophic response functions with the corresponding autotrophy (ζ) and heterotrophy (1-ζ) fractions:

$$f'_T = \zeta f_T(Q10_A) + (1-\zeta) f_T(Q10_H) \tag{17}$$

where $Q10_A$ and $Q10_B$ are the Q10 values for autotrophs and heterotrophs (Table 4).

4.2. Parameterization

4.2.1. Algae and mixotrophs

Parameterization of processes for the algal and mixotrophic groups was based on recent trait-based studies, which consider size as a fundamental trait, but recognize also the taxa-specific differences.

- These parameters were estimated allometrically using the biovolume-weighted average cell volume calculated for each group (Table 6). For A_L, which is mainly composed of diatoms (Table A2), we used the scaling coefficients specifically for freshwater diatoms found by Litchman et al. (2009). For the other groups, we use the coefficients given by Edwards et al. (2012). Cell-specific values were converted to C-specific values by allometrically scaling the carbon contents using the coefficients provided by Menden-Deuer and Lessard (2000). Crane and Grover (2010) suggested Q_{min} of mixotrophs should be 20% higher due to costs of maintaining the organismal apparatus required for herbivory. Here we generalize this by assuming $Q^{real}_{\min} = Q_{\min} + (Q_{\max} - Q_{\min})(1-\zeta)$ (after estimating Q_{max} from Q_{min}, see below), such that at $\zeta = 0$, $Q^{real}_{\min} = Q_{\max}$, i.e., pure herbivores are homeostatic.
- Compared to other parameters, significant allometric relationships for phosphorus-Q_{max} are scarce. Data set collected by Litchman et al. (2009) for marine diatoms suggests scaling coefficients for phosphorus-Q_{max} to be almost identical to that of Q_{min}, i.e., Q_{max} being proportional to Q_{min} with a proportionality constant of $Q_{max}/Q_{min} = 10^{-9.32+10.6} = 19.05$. Considering typical values used in literature (e.g., Gal et al., 2009), we assumed a more modest storage capacity of $Q_{max}/Q_{min} = 10$.
- Given the average volumes and the taxa of the species involved in these groups (3), first the μ_{max} values were visually determined from Edwards et al. (2012), Fig. 3C, to be $10^{0.1}$(=1.1), $10^{-0.1}$(=0.9) and $10^{-0.25}$(=0.55) respectively for A_s, A_l, and M (for the reference temperature: 20° C). Maximum growth rates for A_{pr} was determined to be 0.35, considering relatively low growth rates (Bright and Walsby, 2000). Then, μ_∞ values were calculated using these μ_{max}, allometrically calculated Q_{min} and Q_{max}, and the property $\mu_{max} = \mu_\infty(1 - Q_{min}/Q_{max})$.
- We could not find any significant allometric relationship for K_U (regarding phosphorus uptake), therefore we adjusted these parameters taking into consideration the taxonomical averages reported by Edwards et al. (2012), Fig. 4E.
- There does not seem to exist a significant allometric relationship for the parameters regarding light utilization, therefore corresponding parameters were determined based on taxonomic statistics provided by Schwaderer et al. (2011), Fig. 1.

4.2.2. Zooplankton

- Average biovolume-weighted cell volume of the mixotrophs, M, is 1.3×10^3 μm^3 (Table 1). Considering the species composition of zooplankton groups (Table A1) and body volume for individual species (e.g., Hansen et al., 1997), we estimate the average volume of Z_H and Z_C respectively to be 10^7 and 10^8 μm^3. We then allometrically scale G_{max} of mixotrophs and zooplankton, respectively using the coefficients for flagellates and for all herbivore groups provided by Hansen et al. (1997), as listed with converted units in Table 6.
- Hansen et al. (1997) did not find systematic relationships between K_G and body size or taxanomic group and report an average of 240 mgC m^{-3} = 20 mmolC m^{-3} which we take for all heterotrophs (M, Z_H, Z_C).
- was set for each heterotroph from the relationship ϵ^C =GGE/NGE(Straile, 1997), where GGE refers to gross growth efficiency and NGE refers to net growth efficiency. GGE's were taken from Straile (1997) to be 0.40, 0.3 and 0.3 respectively for M, Z_H and Z_C; and NGE (growth/(growth+metabolic losses)) was estimated to be $NGE = G_{max}/(G_{max} + m + e)$.
- Preferences $p_{j,k}$ were set (Table 5) based on knowledge about the feeding interactions in general and in Lake Bourget when available.
- Unlike the autotrophs, zooplankton are homeostatic (Hessen et al., 2013). The plankton model described above acts homeostatically when $Q_{min} = Q_{max}$, values of which, for herbivores and carnivores are respectively based on *D. longispina* and as an approximate average of *Heterocope* and *Acanthodiaptomus* (Andersen and Hessen, 1991).

4.2.3. Other parameters

- Particulate matter in the water column increases the absorption of light. Different phytoplankton species and detritus have been observed to have different specific-light extinction coefficients. Oubelkheir et al. (2005) suggests 0.02 m^2 mmolC^{-1} for non-algal particles, i.e., *POC* here (which was estimated from *POP* assuming the Redfield ratio). The same study provides a range from 0.012 to 0.045 m^2 mmolC^{-1} for various phytoplankton species, but for the sake of simplicity, we assume here a value of 0.03 m^2 mmolC^{-1} for all phytoplankton species.
- In order to account for the temperature dependence of reaction rates, Q10-rule was employed in this study, for which, the coefficients were taken from Eppley (1972) for autotrophs and Hansen et al. (1997) for heterotrophs (Table 4). For bacteria, Q10 coefficient (used only for remineralization of organic matter r) was assumed to be identical to that of autotrophs. Especially phytoplankton is known to be inhibited at high temperatures (Butterwick et al., 2005), but we had to ignore temperature inhibition in this study, as we are lacking the data required to parameterize such functions (e.g., Jöhnk et al., 2008).

Remaining parameters were either set to values commonly used in similar modelling studies (r,e,m) or manually adjusted based on the qualitative knowledge (w,p_{jk},m^q).

4.3. Physical model

GOTM is a 1-D hydrodynamic model of a water column based on the Reynolds-averaged Navier-Stokes equations and a repository of turbulence closure models. Details about GOTM can be found in Burchard et al. (2006). For the application of GOTM to Lake Bourget, eddy diffusivity was calculated using k-ϵ closure using default model parameters. Air-water fluxes were calculated according to the bulk formula of Kondo (1975) and back-radiation was calculated according to Bignami et al. (1995). All the required atmospheric forcing data were provided in hourly resolution. Short wave radiation was calculated by GOTM as a function of cloud cover, solar altitude and albedo correction (Payne, 1972) as described by Rosati and Miyakoda (1988).

In GOTM, the only source term for heat arises from the attenuation of the shortwave radiation I across the water column, described as the sum of photosynthetically non-active and active radiation:

$$I(z) = I_0 a e^{-\frac{z}{\eta_1}} + I_0(1-a)e^{-\frac{z}{\eta_2} - \int_z^0 \sum_i k_{c,i} c_i(z')dz'} \quad (18)$$

where I_0 is the short wave radiation at the surface, a is the weighting parameter for the differential attenuation of the red and blue-green wavelength components of the light spectrum, η_1 and η_2 are the corresponding absorption length scales, and c_i (as in Eq. (1)) and $k_{c,i}$ are, respectively the concentration and the specific extinction coefficient of item i, constituting the feedback of the coupled bio-

Table 6
Allometric scaling coefficients for U_{max}, Q_{min}, G_{max} (of form $10^a V^b$) and Q^C (of form aV^b). U_{max} and Q_{min} from §:Edwards et al. (2012) þ:Litchman et al. (2009); Q^C from Menden-Deuer and Lessard (2000), where †: protists<3000 μm^3; ‡: diatoms >3000 μm^3; ł: dinoflagellates; G_{max} from Hansen et al. (1997) for the original units of /h, where ð: all flagellates, đ: all groups.

	U_{max}		Q_{min}		Q^C		G_{max}	
X_i	a	b	a	b	$\log_{10}a$	b	a	b
A_S	−8.4	0.81 §	−10.5	0.86 §	−0.583	.860 †	–	–
A_{PR}	−8.4	0.81 þ	−10.5	0.86 þ	−0.583	.860 †	–	–
A_L	−7.65	0.45 §	−10.9	1.0 §	−0.933	.881 ‡	–	–
M	−8.4	0.81 §	−10.5	0.86 §	−0.353	.864 ł	0.3	−0.3 ð
Z_H, Z_C	–	–	–	–	–	–	−0.04	−0.16 đ

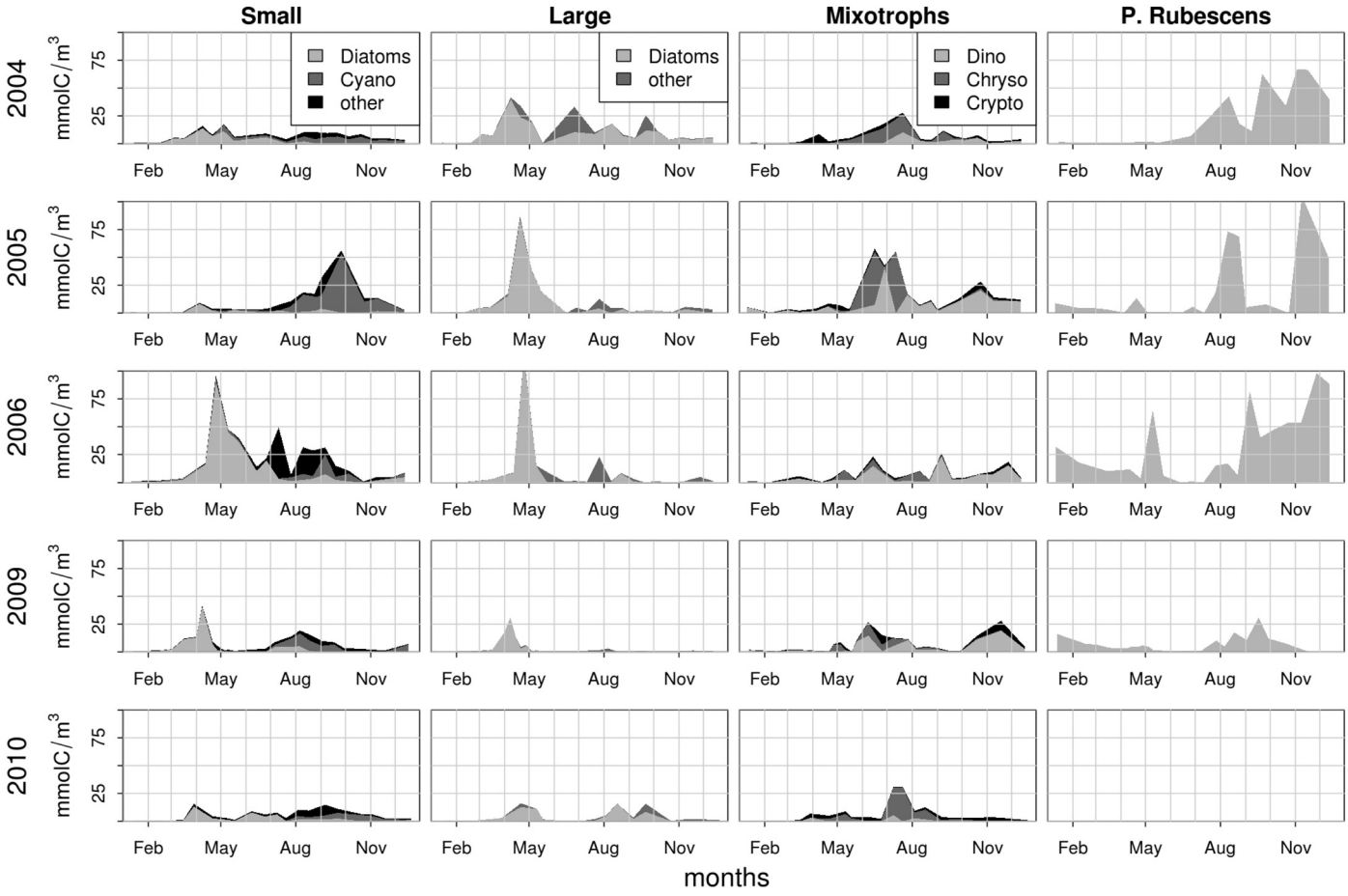

Fig. 3. Measured contribution of major taxonomic classes to each phytoplankton group throughout the simulated years.

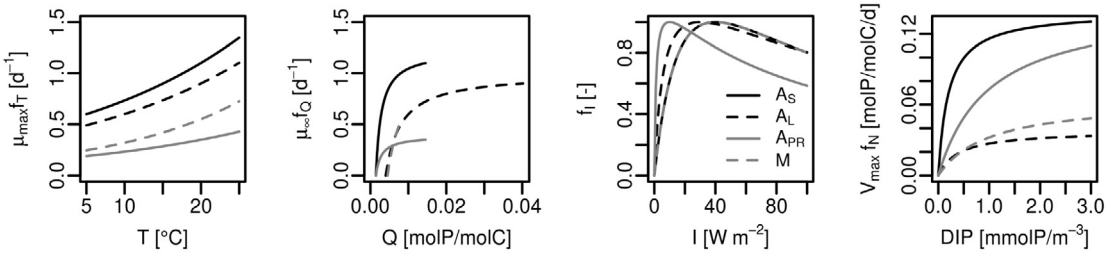

Fig. 4. Limitation functions and their effects on autotrophic functions for each plankton group with the parameter values listed in Tables 3–Table 4. f_T, f_Q, f_I and f_N stand for temperature limitation (Eq. (16)), nutrient limitation of biomass growth (Eq. (3)), light limitation of photosynthesis (Eq. (5)) and nutrient limitation of uptake (Eq. (8)), respectively.

logical model to the physical model. The second term in Eq. (18) corresponds to I_{PAR} (in Eq. (5)). To account for the background turbidity due to suspended material not explicitly accounted for by the model, Jerlov-IA optical class was assumed, corresponding to $a = 0.62$, $\eta_1 = 0.6$ and $\eta_2 = 20$ (Paulson and Simpson, 1977).

4.4. Model coupling and operation

The biological model was developed within the Framework of Aquatic Biogeochemical Models (FABM Bruggeman and Bolding, 2014). FABM acts as an interface between the biogeochemical model and physical model, GOTM which acts as the host of the biological model, by performing the numerical integration of the advection-diffusion-reaction equations (Eq. (1)). According to the on-line coupling scheme employed; state variables of the biogeochemical model are advected based on the the settling rates (ω in Eq. (1)) specified by the biogeochemical model and vertical diffusion rates as a function of eddy diffusivity (K_z in Eq. (1)) and vertical gradients (Eq. (1)); ambient water temperature (T) and (I_{PAR}) estimated by GOTM is provided to the biological model; and in return, absorption of heat (Eq. (18)) is influenced by the concentration of the biological state variables. Through the GOTM-FABM coupler interface (a Fortran namelist file), discretization scheme for advection was chosen as the ULTIMATE QUICKEST algorithm and the source-sink dynamics was chosen to be discretized by the 4th order Runge-Kutta scheme. Simulations were ran with an integration time step of 300 seconds and a vertical resolution of 1 m. Changing the vertical resolution to 0.5 m and time step to 100 seconds was observed to make no difference.

A number of processes that are required for an accurate simulation of the winter mixing are not resolved by the coupled physical-biological model system. These include the variation of the mass and energy content of each vertical layer with depth (i.e., lake hypsography), benthic-pelagic exchange at the lake bottom, various overwintering strategies of plankton, and the pressure sensitivity of the gas vesicles of *P. rubescens*, which determine their ability to regulate their buoyancy later in the season (which itself is also not resolved anyway).Therefore, simulations were started each year shortly before the onset of stratification, precisely on a date when field data that can be used as initial conditions exist. For the initial conditions for temperature, vertically resolved profiles were used. For the initial phytoplankton and zooplankton concentrations, i.e., $X^C_{i,0}$, for which only integrated data respectively from top 20 m and 50 m are available, we assumed that the measured concentrations were homogeneous throughout the water column. For the initial concentration of dissolved nutrients, i.e., DIP_0, no difference was observed between using vertical profiles and homogeneous distribution (obtained by averaging the vertical profile), so we assumed homogeneous distributions, which facilitated testing the model sensitivity to phosphorus availability in the system. The concentration of initial particulate organic phosphorus, POP_0 was calculated as $POP_0 = TP - DIP_0 - \sum_i X^P_{i,0}$, where TP stands for measured total phosphorus and $X^P_{i,0} = X^C_{i,0} * Q_{\max,i}$ implying that the plankton were at their maximum quota, as a result of being exposed to high nutrient concentrations throughout the winter. For all the biological variables, no-flux boundary condition was assumed both for the surface and bottom of the water column.

4.5. Skill assessment metrics

For evaluating the success of the physical model, we used Taylor & Target diagrams (Jolliff et al., 2009). In Target diagrams, standard deviation normalized model bias (B*), and standard deviation normalized unbiased (calculated from the anomalies around the means) root mean square deviation (RMSD), multiplied by the sign of the difference between the standard deviation of model and observation are mapped on Cartesian coordinates. In Taylor diagrams, correlation coefficients between the observations and simulations, and the standard deviation of the model, normalized to that of the observations (equal at 1) are mapped as, respectively, the angle and radius on polar coordinates.

5. Results

Temporal occurrence and taxonomic composition of each phytoplankton group for the simulated years are shown in Fig. 3. Occurrence of the small algae, A_S do not seem to follow a systematic pattern: while in 2006 and 2009, this group, represented mainly by small diatoms, was the major contributor of the spring blooms, in 2005, mainly consisting of cyanobacteria, they were responsible for an intense autumn bloom and finally in 2004 and 2010 this group made up a relatively low and stable background algal biomass throughout the year. A_L were in most years responsible for the spring blooms with a major contribution by diatoms, but in 2004, they were abundant also throughout the summer and autumn. Majority of mixotrophs, M, appeared in summer, without any obvious systematic pattern with regard to their taxonomic constituents.

Phytoplankton growth and limitation functions with the parameters specified for each group listed in Table 3 are shown in Fig. 4, facilitating a comparison between the groups and understanding the succession patterns shown in Fig. 3. A_S is characterized by highest growth rate and nutrient uptake rates, partially explaining its abundance in spring and autumn. A_L also has relatively high growth rates, but it has significantly slower nutrient uptake rates, explaining its absence in summer. A_{PR} is characterized by the lowest growth rates, explaining its delayed growth in the season in most years, and lowest light requirements and greatest high-irradiance intolerance explaining its growth in deeper layers (Jacquet et al., 2014b). M grow almost as slow as the A_{PR}, and is poor in both light and nutrient acquisition.

Seasonal and spatial distributions of the state variables estimated by the model are in general reasonable, as exemplified for the year 2004 in Fig. 5. As the surface waters warm and thermal stratification develops at around mid-March, the mixed layer becomes confined to the surface layers. This relieves phytoplankton from light limitation, leading to blooms of rapid growing A_S and A_L, and consumption of DIP within the mixed layer. Phytoplankton growth fuels mixotrophs and herbivorous zooplankton, leading to POP production and consequently further growth of mixotrophs. Increasing abundances of herbivorous zooplankton and mixotrophs result in a summer-bloom of carnivorous zooplankton, suppressing, in turn, herbivory and hence, preventing the collapse of A_S. Autumn is dominated by *P. rubescens*, which has been growing since mid-summer and at increasingly deeper layers, reaching to about 15–20 meters towards the end of autumn. The season ends with stratification gradually weakening and mixed-layer extending back to deeper layers.

Comparison of measured and model-estimated concentrations of individual plankton groups, and of water temperature, dissolved inorganic phosphorus, total phytoplankton ($\sum_i A_i$), mixotrophs, total zooplankton ($\sum_i Z_i$), and total phosphorus ($= DIP + POP + \sum_i A_i + M + \sum_i Z_i$); all averaged across the top 20 meters of the water column are provided in Figs. 6 and Fig. 7. The visual comparisons for the same set of variables are complemented by Taylor-Target diagrams (Fig. 8). For the case of water temperature, DIP and TP, for which, depth-resolved data are available, Taylor-Target diagrams made with point-wise comparisons for 0–80 m are given in Fig. 9.

The match between the measured and simulated water temperatures is outstanding. For DIP in the top 20 meters, the spring draw-down, and late-spring replenishment in some years was reproduced, although the latter was underestimated in 2010. The gradual withdrawal of TP throughout the season is also well reproduced. Slightly higher model estimations at the beginning of the simulations reflect uncertainties regarding the phosphorus content of the cells, which we assumed to be at Q_{max}, and the value of Q_{max} especially for *P. rubescens*, which is usually the most abun-

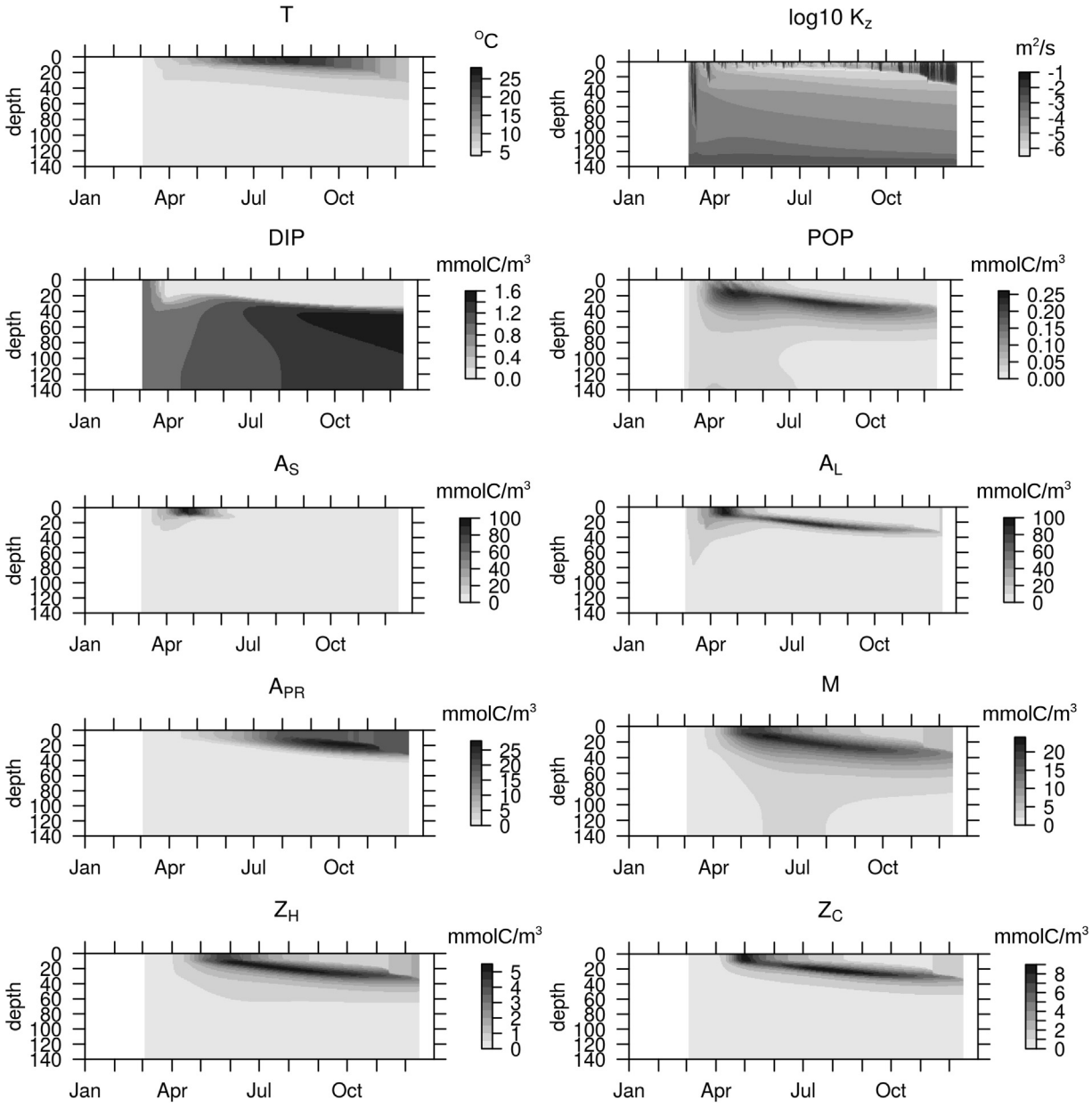

Fig. 5. Spatio-temporal distribution of simulated major variables in 2004.

dant species in the system by the end of winter. Skill metrics for both DIP and TP calculated for the upper 20 m are good (Fig. 8), characterized by near-zero model bias and correlation coefficients at around 0.8.

Model estimates of the lumped plankton groups, namely the phytoplankton, mixotrophs and zooplankton are slightly better than those of individual groups, indicated by lower normalized bias, and modeled variability closer to the observations (Fig. 8). Annual average abundance of all groups are reasonably predicted by the model, indicated by low model bias (Fig. 8). The model also provides a decent estimate of seasonal succession, although some events are reproduced with delays, resulting in phase errors, hence relatively low correlation coefficients and large unbiased RMSD. This is especially true for A_S. An ubiquitous difference between the measured and simulated plankton abundances is the frequency of temporal fluctuations: the simulated trajectories are substantially smoother than the observations, such as those for *P. rubescens*. Inter-annual variability is present in model estimations for some variables, but for some others, like the mixotrophs and the Z_H, the model seems to be repeating an identical seasonal cycle each year. Seasonal amplitudes of Z_H, M and A_{PR} were underestimated, whereas that of A_S was overestimated, leading to lower standard deviations in comparison to the observations.

Vertical distribution of particularly water temperature, but also the DIP and to a lesser extent, TP are realistically represented, as indicated by the relatively high skill scores attained by the point-wise comparisons (Fig. 9). Depth of the mixed layer, and its seasonal changes throughout the year are accurately represented by the model (Fig. 10). Although the very high nutrient concentrations within the last 10 meters of the water column are not captured (not shown), and the nutrient concentrations at the surface are slightly underestimated, the general features, like the depth of the nutrient-depleted layer and the difference between the DIP concentrations at deeper layers in 2004 and 2010 are reproduced reasonably well (Fig. 10). Relatively low skill score attained by TP seem to be caused

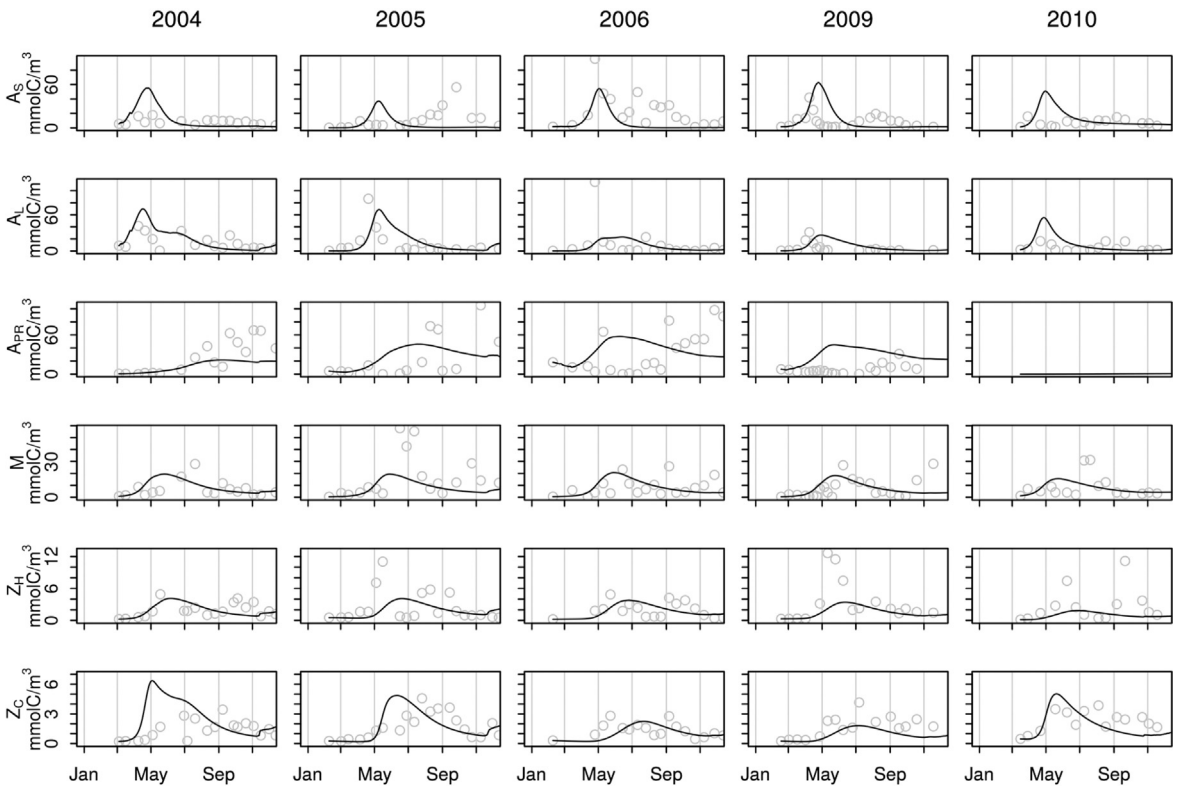

Fig. 6. 0–20 m averaged concentration of simulated (lines) and measured (circles) concentration of plankton groups.

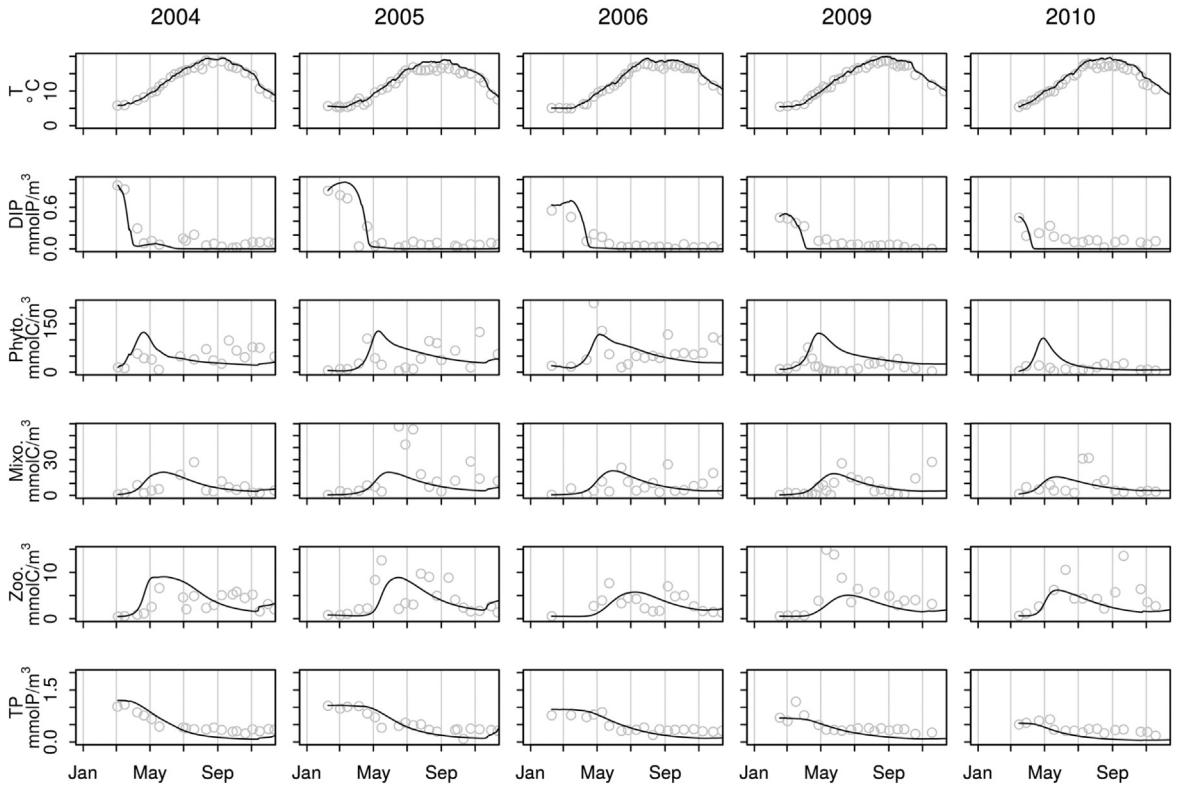

Fig. 7. 0–20 m averaged concentration of simulated (lines) and measured (circles) concentration of biological variables.

by an unrealistic accumulation of organic material near the thermocline (Fig. 10), which is mainly driven by A_{PR}, A_L and M (Fig. 5).

In Jacquet et al. (2014b), it was hypothesized that, among others, two important factors for the disappearance of *P. rubescens* in Lake Bourget in 2010 was decreasing winter-phosphorus con-

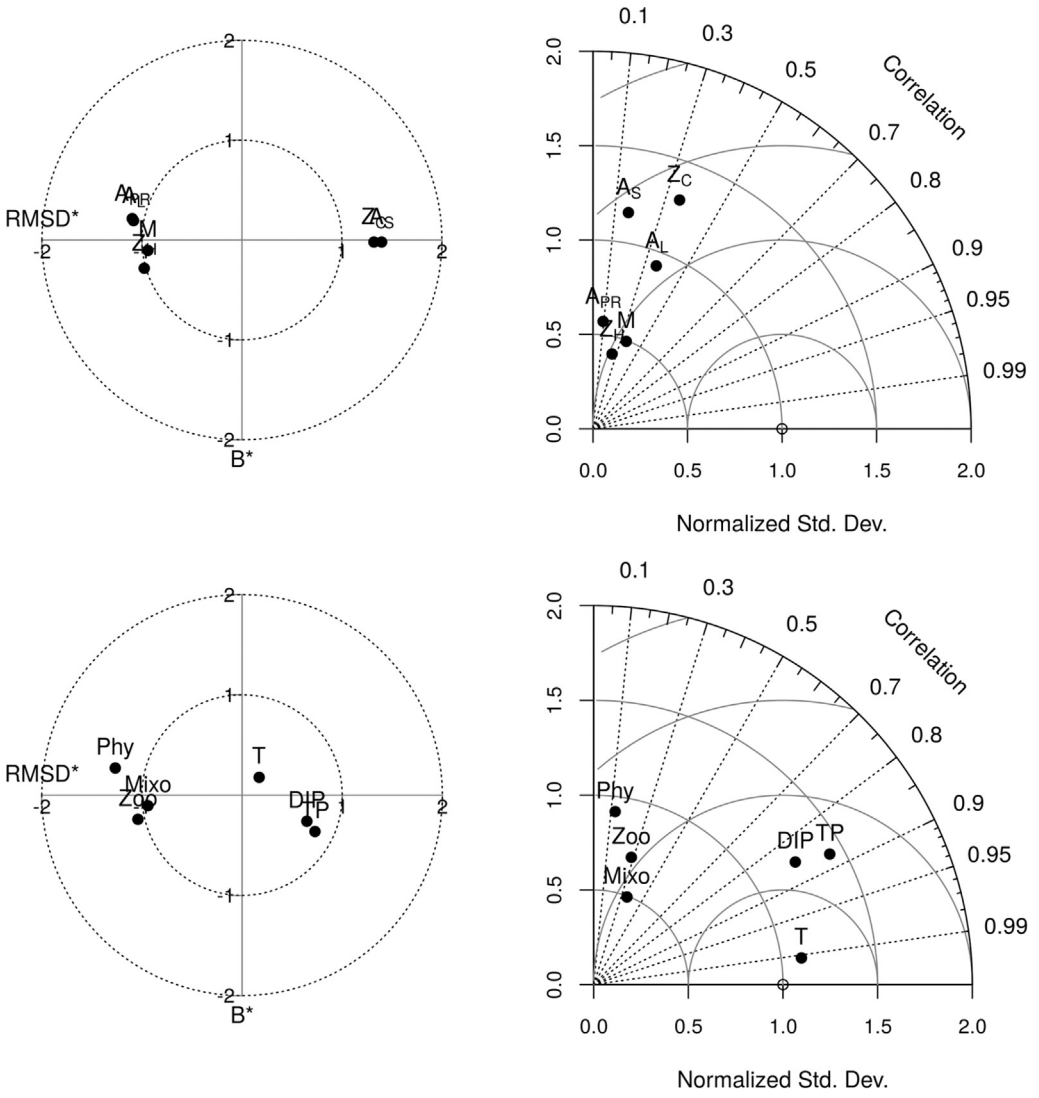

Fig. 8. Target-Taylor diagrams for 0–20 m average concentration of (top) individual plankton groups and (bottom) dissolved phosphorus and total phosphorus, total phytoplankton, total mixotrophs and total zooplankton carbon biomass.

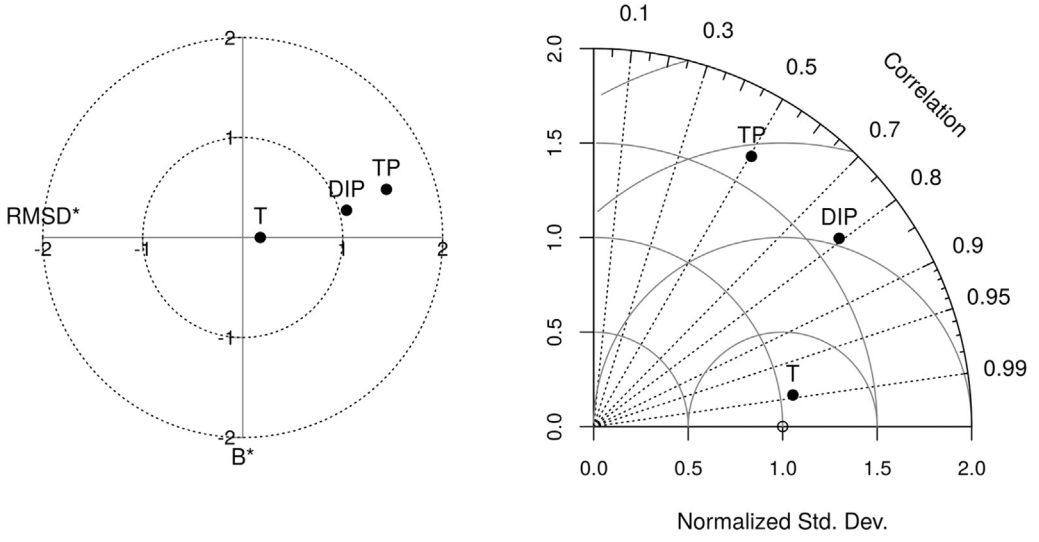

Fig. 9. Target-Taylor diagrams for temperature, dissolved phosphorus and total phosphorus within the upper 80 m, depth-resolution retained, unlike in Fig. 8gr9

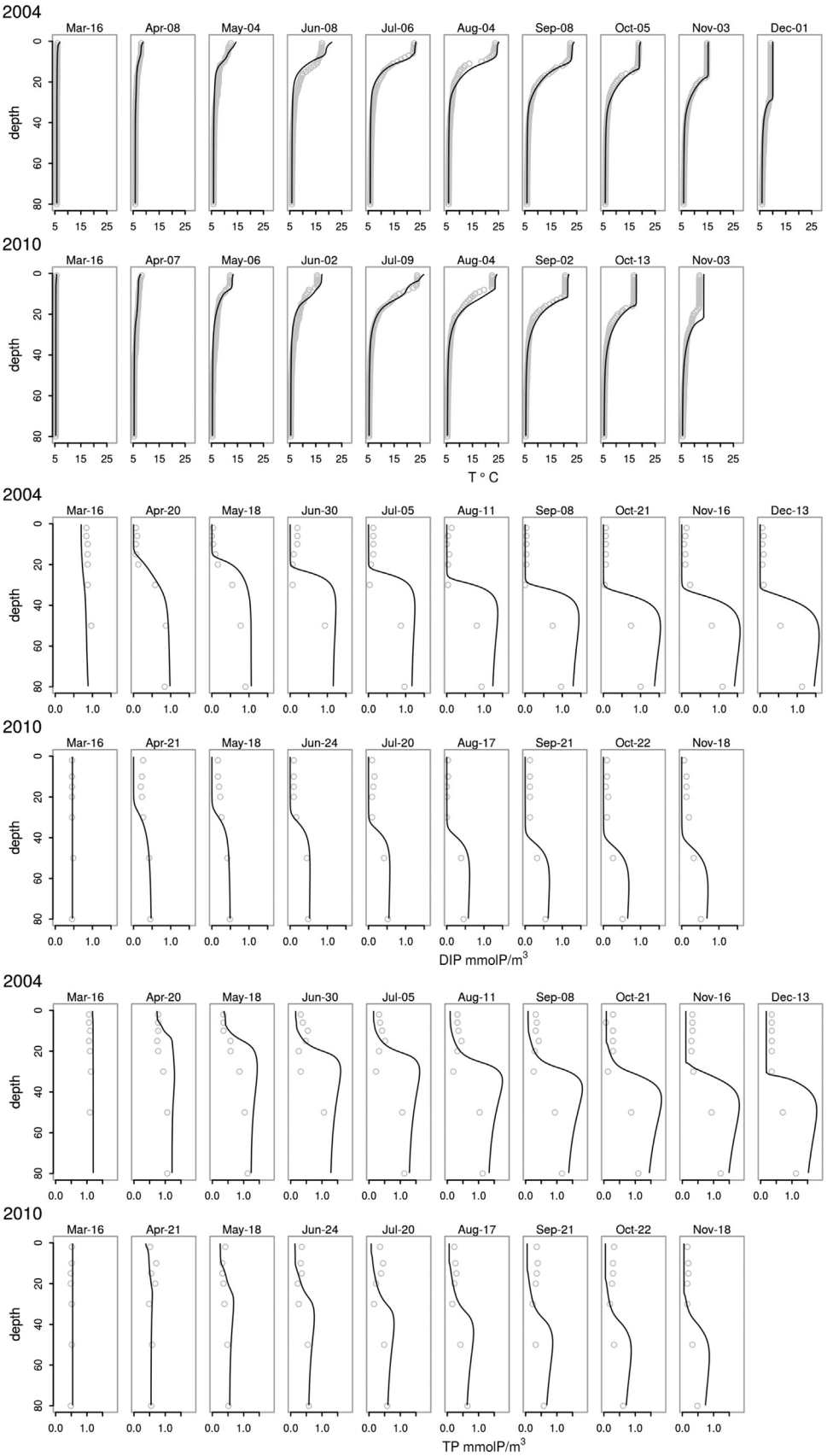

Fig. 10. Simulated (lines) and measured (circles) Temperature, DIP and TP profiles from 2004 and 2010 within the upper 80 m. Only the first measurements in each month are shown. Profiles from identical months in different years are aligned.

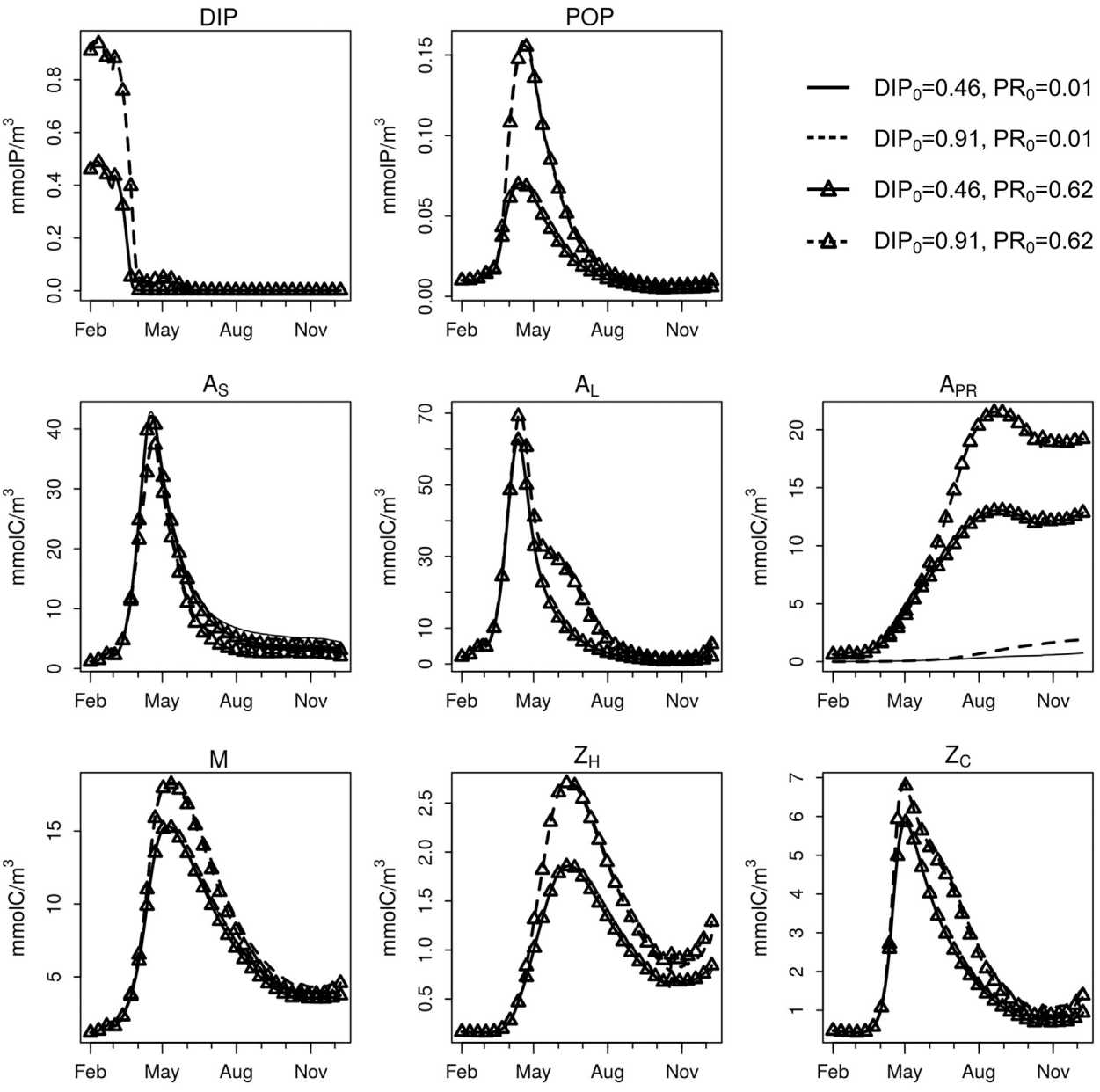

Fig. 11. Surface (0–20 m) average water column average state variables with initial DIP concentration of DIP_0 = 0.46 mmolP m^{-3} as in 2010 (solid lines), DIP_0 = 0.91 mmolP m^{-3} as in 2004 (dashed lines), in combination with initial *P. rubescens* concentration of PR_0 = 0.01 mmolC m^{-3} as (was assumed) in 2010 (no marker) and PR_0 = 0.62 mmolC m^{-3} as in 2004 (triangles). Initial conditions for all other variables and meteorological forcing was as in 2010.

centrations and too small winter inoculum. Despite the fact that no *P. rubescens* was detected in the phytoplankton assemblages throughout the year 2010, the model was initiated with a winter inoculum of 10^{-2} mmolC m^{-3}, which is close to the minimum observed concentration in 2004. Starting from this small inoculum, *P. rubescens* biomass did not grow substantially (Fig. 6)). In order to gain some insight into the reasons that eliminated *P. rubescens* from the system, a scenario analysis was performed, where the initial, winter concentrations of *P. rubescens* and DIP were replaced with the values observed in 2004 (Fig. 11). Higher initial DIP (0.91 instead of 0.46 mmol/m^3) resulted in slightly higher *P. rubescens* concentrations, although the difference was not appreciable. On the other hand, higher winter inoculum (0.62 instead of 0.01 mmol/m^3) resulted in larger than 10 mmol/m^3 of *P. rubescens* during autumn. Setting both the DIP and A_{PR} concentrations to 2004 values resulted in dynamics very similar to those obtained in 2004, suggesting that other differences between these two years, e.g., with respect to the meteorological conditions and initial concentration of other plankton groups, were not critical in determining *P. rubescens* dynamics.

6. Discussion

In this study, we described a novel biogeochemical model coupled to a 1-D hydrodynamical model, and its application to Lake Bourget. We demonstrate that the model is able to provide a reasonable representation of the seasonal phosphorus cycle and to some extent, the succession of the plankton groups in this ecosystem. Our scenario analysis suggests that the winter concentration of *P. rubescens* has a determining role for its dynamics in the following growth season.

The model is implemented as three FABM (Bruggeman and Bolding, 2014) modules, which can be coupled at run-time (i.e., without the need for changing and re-compiling the model code): a nutrient module, a detritus module, and a plankton module that can

be placed anywhere along the autotrophy-heterotrophy continuum (Flynn et al., 2012) with the 'autotrophy fraction' parameter ζ, enabled by a generalized formal description of autotrophic and heterotrophic processes (Section 4.1). In the present implementation, the plankton module is coupled six times to describe interactions of three purely autotrophic, two purely heterotrophic and a mixotrophic plankton groups. Realistic representation of spatio-temporal distribution of inorganic and particulate phosphorus, as well as the plankton groups constitute a proof of the concept. These generic modules thus enable description of various food web configurations in run-time and therefore can facilitate site-specific configurations in future studies.

Incorporation of mixotrophy is another novel aspect of the current study, given that mixotrophy has been, with exceptions (e.g., Ward and Follows, 2016), neglected in ecosystem scale model applications. Here, the description of mixotrophy is quite simplistic, relying on the assumption that there exists a linear trade-off between autotrophic and heterotrophic abilities (Crane and Grover, 2010), and the assumption that the parameters of heterotrophic and autotrophic traits reflect the conditions that enforced pure heterotrophy or autotrophy in the meta-analysis data that formed the basis for parameterization in this study. It should be further noted that, in reality, a major carbon and nutrient source for mixotrophs is often bacteria (Mitra et al., 2014), which is not explicitly modelled in this study, but is implicitly represented by the POM pool, P content of which is known, but C content is assumed to be proportional to P by the Redfield ratio. Further resolution of the microbial loop and the organic matter pools in Lake Bourget would be out of the scope of the current study, but constitutes a potential future goal, as with ongoing oligotrophication, relative importance of mixotrophs in the system can be anticipated to increase (Kamjunke et al., 2007; Mitra et al., 2014).

In this study, mixotrophs and herbivorous and carnivorous zooplankton were assigned as individual functional groups based on their position in the food web. *P. rubescens* was assigned as a separate algal group because of its distinctive eco-physiology characterized by low-light tolerance (Walsby and Schanz, 2002), slow growth (Bright and Walsby, 2000), and grazing defense (Kurmayer and Jüttner, 1999) as well as the fact that it represented about half of the phytoplankton assemblage in some years ( ). Previous modelling studies focusing on similarly *P. rubescens*-infested lakes unequivocally assigned *P. rubescens* an own group (Omlin et al., 2001; Copetti et al., 2006; Mieleitner and Reichert, 2008; Carraro et al., 2012). Remaining phytoplankton were separated by size, forming 'small' and 'large' algal groups, given the importance of size in determining light and light utilization traits, among others (Finkel et al., 2010). There exist modelling studies where taxonomic classes were parameterized directly as functional groups (e.g., Jöhnk et al., 2008; Carraro et al., 2012), but categorization based on size, thereby combining different taxonomic classes within a given functional group like in this study is not uncommon (e.g., Mieleitner and Reichert, 2008; Gal et al., 2009; Rinke et al., 2010).

Parameterization of the plankton groups was largely based on allometric relationships and taxonomic properties, inspired by recent meta-analyses (Litchman et al., 2009; Schwaderer et al., 2011; Edwards et al., 2012). This approach was to some extent necessary, due to the lack of information on physiological parameters of the specific plankton species or groups observed in Lake Bourget. On the other hand, we believe that this approach should produce a more consistent and transferable (i.e., applicable to other systems) parameter set than that could be obtained by a pure calibration exercise, which is problematic due to poor parameter identifiability of plankton functional group models (Anderson, 2005; Mieleitner and Reichert, 2008). In this study, parameter tuning was restricted to parameters like zooplankton preferences, sinking rates (of A_L and detritus) and remineralization rates. Setting zooplankton feeding preferences is a common problem in ecosystem models, as model results are sensitive to different parameterizations (Gentleman et al., 2003), and as the experimental data so far are based on specific prey-predator pairs that are hardly generalizable. For the parameterization of sinking and remineralization rates, we acknowledge potential biases in the form of an underestimation of sinking rates and an overestimation of remineralization rates to compensate the lack of river nutrient fluxes.

Based on the classical variable internal stores model schemes, the storage capacity, Q_{max}/Q_{min} has been shown to have a critical importance in the presence of temporal (Grover, 1991) and/or spatial (Kerimoglu et al., 2012) heterogeneity. Different allometric scalings observed in Q_{max} and Q_{min} for nitrogen, contrasting with similar coefficients in those for phosphorus have been suggested to explain marine diatoms being larger than freshwater diatoms (Litchman et al., 2009). On the other hand, it is questionable whether Q_{max} should be considered as a fixed physiological parameter, as the observed maximum nutrient contents in phytoplankton cells might as well be reflecting the acclimative down-regulation of the uptake rate, which depends on the specific settings, like limitation by other nutrients, supply rates and light limitation, as shown by optimality based model schemes (Pahlow et al., 2013; Wirtz and Kerimoglu, 2016). This might be the reason for lack of robust patterns in distributions of Q_{max} across cell size or taxa, hence, its exclusion from analyses aiming to identify allometric and taxonomic variations in physiological traits (e.g., Litchman et al., 2007; Edwards et al., 2012). In this study, acknowledging the poor understanding of the issue, we assumed a fixed proportionality between Q_{max} and Q_{min}, in order to avoid introducing a potentially strong but unjustified trait that can effect the competitive outcomes.

Overall, the model performance is good, given the limitations of the idealized 1-D approach. Model estimates for water temperature are almost excellent (Figs. 7–10). Average surface concentrations of DIP and TP can considered to be very good ($r > 0.85$, Fig. 8). The measured DIP concentrations during summer tend to be somewhat higher than the simulations, which might be, to some extent, due to the river fluxes that not represented by the model, however, considering the long water residence time of the lake (about 10 years) there is probably some other mechanism involved. Vertical profiles of DIP, and to a lesser extent, TP within the upper 80 m are quite realistically reproduced by the model. Annual average concentration of plankton groups are well reproduced, indicated by low bias, but the seasonal dynamics is poorly represented, resulting in phase errors, and low correlation coefficients (Fig. 6). Interannual variability of the data is also more pronounced than that of the simulations. Especially *P. rubescens* follows contrasting patterns in different years: in the form of smooth patterns in 2004 and 2009, and very rapid changes in the years 2005 and 2006, which are likely to be related with some vertical or lateral transport mechanism like those induced by internal waves or upwelling events that occur frequently in Lake Bourget (Cuypers et al., 2011), given their low growth rates (Bright and Walsby, 2000) and limited losses imposed by zooplankton (Kurmayer and Jüttner, 1999). On the other hand, their growth at 10–20 m depth (Fig. 5) notably coincides well with the observations in Lake Bourget (Jacquet et al., 2005, 2014b; Le Vu et al., 2011). In reality, this phenomena is usually attributed to buoyancy regulation (Walsby et al., 2004), whereas in this study, no active mobility mechanism has been considered and their sub-surface growth largely reflects the parameterized low-light tolerance and high-light inhibition of the species (Walsby and Schanz, 2002). The depth-dependent mortality we assumed for *P. rubescens* (Eq. (14)) does not play a significant role in the occurrence of such thin layers, whereas it certainly pulls the depth of maximum concentration a few meters upwards. Our preliminary work (not shown) suggest that the thin-layers can be represented by specifying an optimum growth temperature or irra-

diance, however, using a process-based buoyancy regulation model (e.g., Kromkamp and Walsby, 1990) would be more useful for gaining a better understanding of the relevance of the formation of thin layers. Finally, high frequency fluctuations in other variables are not captured, which might be related with extreme river discharge events (Vinçon-Leite et al., 1995) in the system. A 3-D modelling study revealed that in a relatively smaller (surface area: 5 km^2) Lake Pusiano, a major flood event caused a significant variation in the horizontal distribution of *P. rubescens* (Carraro et al., 2012). Given that the two major tributaries of Lake Bourget are in the South (Bryhn et al., 2010), and the outflows are in the North, such can be expected in Lake Bourget as well to some extent, but the effects are presumably smaller due to the much smaller quantity of fluxes in relation to the water volume in Lake Bourget in comparison to Lake Pusiano, which has a water residence time of about 1 year (Carraro et al., 2012), i.e., one tenth that of Lake Bourget.

Occurrence of *P. rubescens* is usually attributed to the nutrient availability, when long-term dynamics (Dokulil and Teubner, 2012; Posch et al., 2012) and lakes at different trophic states are considered (Salmaso et al., 2012; Anneville et al., 2015). Within our study period, winter DIP fell from 0.9 to 0.46 mmolP/m^3 (corresponding to 27.9 to 14.3 mgP/m^3) between 2004 and 2010 (Fig. 1), which does not encompass a large range relative to the above examples. Indeed, our scenario analysis where we used the winter DIP concentration of 2004 for simulating 2010 did not result in a significant difference from the reference simulation of 2010 (Fig. 11). In contrary, when the winter concentration of *P. rubescens* in 2004 was used for simulating 2010, a large *P. rubescens* bloom was formed, unlike the reference simulation of 2010 (Fig. 11). These results suggest that the initial abundances by the end of the winter are highly important for the dynamics of *P. rubescens* within the growth season, which is in line with the findings of Jacquet et al. (2014b), who showed a significant relationship between the winter-spring, spring-summer and summer-autumn biomasses. Qualitatively the same results were obtained when the scenario analysis was repeated with an altered model parameterization (not shown), where, *P. rubescens* was described as a species with slightly stronger resource competition traits (50% lower K_U and 25% higher μ_∞, given the uncertainties of the allometric scaling of these parameters), and slighty weaker defense against predation (mixotrophs feeding on them with $p_{M,k} = 0.5, 0.4$ and 0.1 for k = POM, A_S and A_{PR}, given the lacking evidence for the feeding interactions between *P. rubescens* and mixotrophic species in Lake Bourget).

The sensitivity of growing season *P. rubescens* abundance to the initial population size after winter does not simply result from a delayed geometric growth: when the scenario analysis is repeated with a structurally different model where *P. rubescens* is the only autotroph, i.e., not having any competitors, even the scenario with low initial inoculum and phosphorus concentrations results in a substantial bloom with concentrations reaching up to 50 mmolC m^{-3} (Appendix A.2), which is close to the concentrations observed in the years with intense *P. rubescens* occurrences. These findings therefore suggest that the disappearance of *P. rubescens* from Lake Bourget was actually due to competitive exclusion, facilitated by the phenomena called the priority effect (Hodge et al., 1996), in which, the species with higher initial concentrations outcompete their competitors with lower initial concentrations by making the abiotic environment inhabitable by the others. The priority effect has been previously reported from field measurements (Tapolczai et al., 2014) and mesocosm experiments (Sommer and Lewandowska, 2011). Vertical distributions obtained under different scenarios (not shown) suggest that the priority effect is manifested as a bistability of both phytoplankton composition and vertical distribution of phytoplankton biomass (as in Ryabov et al., 2010). When *P. rubescens* start the season from relatively higher concentrations, they end up being the dominant species starting from summer by forming a dense layer at the metalimnion and thereby prevent the growth of mainly the small species through intensifying the nutrient limitation in the upper layers. To the contrary, when they start from low concentrations, small phytoplankton persist in the surface layers throughout the summer, making it thereby difficult for *P. rubescens* to grow through intensifying light limitation. The self-stabilizing nature of these two alternative states may partially explain the inter-annual variability of the *P. rubescens* abundances commonly observed in various deep lakes (Vinçon-Leite et al., 2002; Salmaso, 2010; Jacquet et al., 2014b; Anneville et al., 2015).

It should be noted that, although the additional *P. rubescens* growth caused by higher initial phosphorus was relatively small, the higher *P. rubescens* concentration by the beginning of winter might be of substantial importance for the dynamics that follow later in the next season, as scenarios with higher initial *P. rubescens* concentrations suggest (Fig. 11). Moreover, the range of phosphorus concentrations in this scenario analysis is relatively small relative to the historical observations in Lake Bourget itself and in other lakes, so it does not imply that phosphorus availability is unimportant for the occurrence of this *P. rubescens*. In contrary, we believe that the long-term decrease of phosphorus in Lake Bourget was a prerequisite for the final disappearance of *P. rubescens* as suggested by (Jacquet et al., 2014b). A model-aided test of this hypothesis can be achieved with a model validated for contrasting conditions with respect to the trophic state and the availability of *P. rubescens* that are observed either in a single lake across a long-term transition, or multiple lakes of different trophic status.

In Lake Bourget (Vinçon-Leite et al., 2002; Jacquet et al., 2014b; Anneville et al., 2015), as well as in other deep lakes like Lake Zurich (Walsby et al., 1998; Posch et al., 2012), Lake Garda (Salmaso, 2010) and Mondsee (Dokulil and Teubner, 2012), the abundance of *P. rubescens* by the end of winter is largely determined by meteorological conditions during winter. In such deep, warm monomictic lakes, cooling in mild winters may end up being insufficient to cause a full overturn, leading to a reduced dilution of the *P. rubescens* concentrations, as well more *P. rubescens* cells survive the winter (Walsby et al., 1998). Beyond the fact that phosphorus reached low concentrations in Lake Bourget, it seems like the coincidence of such a cold winter with a weak autumn population, might be the explanation for the complete elimination of the *P. rubescens* in 2010. Indeed, in 2010, both the autumn and winter air temperatures were among the coldest in the region (Anneville et al., 2015), and *P. rubescens* had a relatively low autumn concentration (Jacquet et al., 2014b, and this study, Fig. 6). In this context, it is worth noting that the warming trend observed in Lake Bourget (Vinçon-Leite et al., 2014) can be expected to further continue given the anticipated warming of especially the winters in the alpine region (Beniston, 2006), possibly promoting the re-establishment of *P. rubescens* in Lake Bourget, given the evidence that warming promoted *P. rubescens* in Lake Zurich (Anneville et al., 2004) and Lake Geneva (Gallina et al., 2017).

In Lake Bourget, mixing does not reach the lake bottom during warm winters, such as in 2007 and 2008, which leads to significantly lower phosphorus concentrations and high *P. rubescens* abundances later in the season season (Jacquet et al., 2014b). Therefore an extended model based analysis of plankton succession encompassing the winter dynamics would be highly relevant. Although the model presented in this study can serve as a starting point, several other processes need to be taken into account, including the lake hypsography, benthic-pelagic exchange, overwintering strategies of plankton, and the buoyancy regulation of *P. rubescens*, as well its inhibition through collapsing of gas vesicles under high pressure. Other rare behavior of *P. rubescens* worth considering in future modelling studies include colony formation

behavior and its effect on predation by zooplankton. In this study, we assumed a non-zero but low preference of *P. rubescens* by the herbivorous zooplankton, but the evidence suggests that the grazing rate depends on the colony size (Oberhaus et al., 2007), and there is a significant relationship between the nutrient status and colony size (Jacquet et al., 2014b), suggesting that this preference should not be constant in time and space.

Acknowledgements

This study is a contribution to the PhyCl project and to the observatory of alpine lakes (OLA). Data were made available by SOERE OLA-IS, INRA Thonon les Bains, CISALB and ecoinformatics ORE-INRA team. Authors are grateful to all the technicians, engineers and researchers who have contributed to the monitoring of Lake Bourget. We thank two anonymous referees for their comments. Funding for OK was provided by the University of Savoie Mont Blanc (AAP 2012). OK was additionally supported by the German Research Foundation (DFG) through the priority program 1704 'DynaTrait'.

Appendix A. Composition of functional groups

A.1 Composition of functional groups

Taxonomic classes and stage classes contributing to each zooplankton group are listed in Table A1. Major phytoplankton species in Lake Bourget making up the top ~ 80 % biovolume of each phytoplankton group, and the taxonomic class they belong are listed in Table A2.

Table A1
Composition of zooplankton groups. Daphnia + Diaphanosoma: *Daphnia Hyalina, Daphnia Galeata + Diaphanosoma brachyurum*; Calanides: *Eudiaptomus gracilis*; Bosmina + Eubosmina: *Bosmina longirostris, Eubosmina longispina, Eubosmina coregoni*; Cyclops: *Cyclops sp., Cyclops vicinus, Cyclops prealpinus, Megacyclops viridis, Mesocyclops leuckarti, Thermocyclops crassus*; Leptodora: *Leptodora kindtii*; Bythotrephes: *Bythotrephes longimanus*.

Species	% contribution
Z_H (% 57.51):	
Daphnia + Diaphanosoma	52.48
Calanoid adults	15.03
Calanoid cl. 4-5	10.91
Calanoid cl. 1-3	1.81
Calanoid nauplii 1-6	0.02
Bosmina + Eubosmina	13.31
Cyclops cl 1-3	6.01
Cyclops nauplii 1-6	0.43
Z_C (% 42.49):	
Cyclops adults	53.02
Cyclops classes 4-5	26.80
Leptodora	17.81
Bythotrephes	2.371

Table A2
2004–2010 average species composition of phytoplankton (A_S, A_L and A_{PR}) and mixotroph (M) groups, separated by horizontal lines.

Species	Tax.group	%BV	$\sum$%BV
Aphanocapsa delicatissima	Cyano	13.93	13.93
Fragilaria crotonensis	Diatoms	13.33	27.25
Cyclotella spp>9μm + Stephanodiscus minutulus >7μm	Diatoms	10.48	37.74
Asterionella formosa	Diatoms	5.72	43.45
Aphanizomenon flos-aquae	Cyano	5.51	48.97
Pediastrum boryanum	Chloro	5.50	54.47
Rhodomonas minuta var. nannoplanctica	Crypto	5.38	59.84
Cyclotella cyclopuncta	Diatoms	4.96	64.80
Aphanocapsa holsatica	Cyano	3.61	68.40
Cyclotella costei	Diatoms	3.29	71.69
Fragilaria ulna var. acus	Diatoms	2.28	73.97
Ankistrodesmus nannoselene	Chloro	2.25	76.22
Erkenia subaequiciliata	Chryso	2.24	78.46
Pseudanabaena limnetica	Cyano	1.98	80.45
Cyclotella bodanica var. lemanensis	Diatoms	22.67	22.67
Diatoma tenuis	Diatoms	17.23	39.90
Mougeotia gracillima	Zygophy.	16.83	56.73
Fragilaria ulna var. angustissima	Diatoms	8.48	65.21
Aulacoseira islandica subsp. helvetica	Diatoms	5.43	70.64
Stephanodiscus alpinus	Diatoms	4.40	75.04
Stephanodiscus neoastraea	Diatoms	4.14	79.18
Chlamydomonas sp.	Chloro	3.72	82.91
Planktothrix rubescens	Cyano	100.00	100.00
Ceratium hirundinella	Dino	25.82	25.82
Dinobryon divergens	Chryso	17.20	43.01
Rhodomonas minuta	Crypto	14.81	57.82
Cryptomonas sp.	Crypto	6.76	64.58
Dinobryon divergens vide	Chryso	5.49	70.07
Dinobryon sociale var. americanum	Chryso	4.75	74.82
Gymnodinium helveticum	Dino	4.44	79.26
Peridinium willei	Dino	3.51	82.76

A.2 Sensitivity of scenario analysis to the model structure

If the disappearance of *P. rubescens* in 2010 is really associated with the 'priority effect' as claimed in the main text, in the absence of its competitors (other phytoplankton groups), *P. Rubescens* should reach to substantial abundances in 2010, even if starting from a small initial abundance after winter. In order to test this prediction, we performed the scenario analysis with an alternative model structure, in which *P. Rubescens* is the only autotroph available in the system, herbivorous zooplankton (ZH) feeds on P. Rubescens and carnivorous zooplankton (ZC) feeds on ZH. Results of the scenario analysis obtained with this simple model structure is qualitatively different than those obtained with the reference model described in the text: initial inoculum of *P. Rubescens* indeed only determines the timing of the bloom, and not the presence/absence (Fig. B1). This analysis suggests that the disappearance of P. Rubescens from Lake Bourget is not a simple linear response to the inoculum size, but a case of competitive exclusion facilitated by the priority effect.

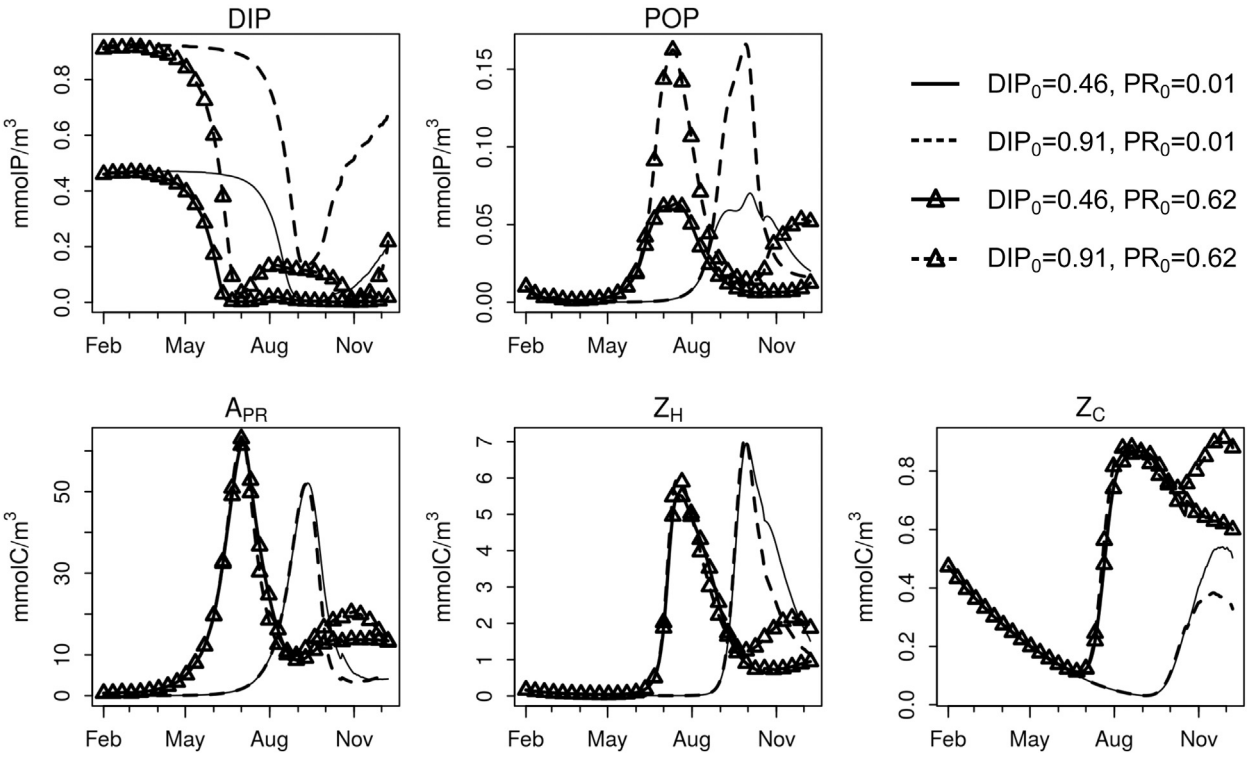

Fig. B1. Surface (0–20 m) average water column average state variables with initial DIP concentration of DIP_0 = 0.46 mmolP m^3 as in 2010 (solid lines), DIP_0 = 0.91 mmolP m^3 as in 2004 (dashed lines), in combination with initial *P. rubescens* concentration of PR_0 = 0.01 mmolC m^3 as (was assumed) in 2010 (no marker) and PR_0 = 0.62 mmolC m^3 as in 2004 (triangles). Initial conditions for all other variables and meteorological forcing was as in 2010.

References

Andersen, T., Hessen, D.O., 1991. Carbon, nitrogen, and phosphorus content of freshwater zooplankton. Limonol. Oceanogr. 36, 807–814.

Anderson, T.R., 2005. Plankton functional type modelling: running before we can walk? J. Plank. Res. 27, 1073–1081.

Anneville, O., Domaizon, I., Kerimoglu, O., Rimet, F., Jacquet, S., 2015. Blue-Green Algae in a "Greenhouse Century"? New insights from field data on climate change impacts on cyanobacteria abundance. Ecosystems 18, 441–458.

Anneville, O., Souissi, S., Gammeter, S., Straile, D., 2004. Seasonal and inter-annual scales of variability in phytoplankton assemblages: comparison of phytoplankton dynamics in three peri-alpine lakes over a period of 28 years. Freshw. Biol. 49, 98–115.

Armstrong, R., 1994. Grazing limitation and nutrient limitation in marine ecosystems: steady state solutions of an ecosystem model with multiple food chains. Limonol. Oceanogr. 39, 597–608.

Beniston, M., 2006. Mountain weather and climate: a general overview and a focus on climatic change in the Alps. Hydrobiologia 562, 3–16.

Berge, T., Chakraborty, S., Hansen, P.J., Andersen, K.H., 2017. Modeling succession of key resource-harvesting traits of mixotrophic plankton. ISME J. 11, 212–223.

Bignami, F., Marullo, S., Santoleri, R., Schiano, M.E., 1995. Longwave radiation budget in the Mediterranean Sea. J. Geophys. Res. 100, 2501.

Briand, J.F., Jacquet, S., Flinois, C., Avois-Jacquet, C., Maisonnette, C., Leberre, B., Humbert, J.F., 2005. Variations in the microcystin production of *Planktothrix rubescens* (cyanobacteria) assessed from a four-year survey of Lac du Bourget (France) and from laboratory experiments. Microb. Ecol. 50, 418–428.

Bright, D., Walsby, A., 2000. The daily integral of growth by *Planktothrix rubescens* calculated from growth rate in culture and irradiance in Lake Zürich. New Phytolog. 146, 301–316.

Bruggeman, J., Bolding, K., 2014. A general framework for aquatic biogeochemical models. Environ. Model. Softw. 61, 249–265.

Bryhn, A., Girel, C., Paolini, G., Jacquet, S., 2010. Predicting future effects from nutrient abatement and climate change on phosphorus concentrations in Lake Bourget, France. Ecol. Model. 221, 1440–1450.

Burchard, H., Bolding, K., Kühn, W., Meister, A., Neumann, T., Umlauf, L., 2006. Description of a flexible and extendable physical-biogeochemical model system for the water column. J. Mar. Syst. 61, 180–211.

Butterwick, C., Heaney, S.I., Talling, J.F., 2005. Diversity in the influence of temperature on the growth rates of freshwater algae, and its ecological relevance. Freshw. Biol. 50, 291–300.

Carraro, E., Guyennon, N., Hamilton, D., Valsecchi, L., Manfredi, E.C., Viviano, G., Salerno, F., Tartari, G., Copetti, D., 2012. Coupling high-resolution measurements to a three-dimensional lake model to assess the spatial and temporal dynamics of the cyanobacterium *Planktothrix rubescens* in a medium-sized lake. Hydrobiologia 698, 77–95.

Chen, B., Liu, H., 2010. Relationships between phytoplankton growth and cell size in surface oceans: Interactive effects of temperature, nutrients, and grazing. Limnol. Oceanogr. 55, 965–972.

Copetti, D., Tartari, G., Morabito, G., Oggioni, A., Legnani, E., 2006. A biogeochemical model of Lake Pusiano (North Italy) and its use in the predictability of phytoplankton blooms: first preliminary results. J. Limnol. 65, 59–64.

Crane, K., Grover, J., 2010. Coexistence of mixotrophs, autotrophs, and heterotrophs in planktonic microbial communities. J. Theor. Biol. 262, 517–527.

Cuypers, Y., Vinçon-Leite, B., Groleau, A., Tassin, B., Humbert, J.F., 2011. Impact of internal waves on the spatial distribution of *Planktothrix rubescens* (cyanobacteria) in an alpine lake. ISME J. 5, 580–589.

Dokulil, M.T., Teubner, K., 2012. Deep living *Planktothrix rubescens* modulated by environmental constraints and climate forcing. Hydrobiologia 698, 29–46.

Droop, M., 1968. Vitamin B12 and marine ecology. IV. The kinetics of uptake, growth and inhibition in *Monochrysis lutheri*. J. Mar. Biol. Assoc. United Kingdom 48, 689–733.

Druart, J.C., Rimet, F., 2008. Protocoles d'analyse du phytoplancton de l'INRA: prélèvement, dénombrement et biovolumes. Technical Report. INRA. Thonon les Bains.

Dumont, H.J., de Velde, I., Dumont, S., 1975. The dry weight estimate of biomass in a selection of Cladocera, Copepoda and Rotifera from the plankton, periphyton and benthos of continental waters. Oecologia 19, 75–97.

Edwards, K.F., Thomas, M.K., Klausmeier, C.A., Litchman, E., 2012. Allometric scaling and taxonomic variation in nutrient utilization traits and maximum growth rate of phytoplankton. Limnol. Oceanogr. 57, 554–566.

Eppley, R., 1972. Temperature and phytoplankton growth in the sea. Fish. Bull. 70, 1063–1085.

Ernst, B., Hoeger, S.J., Brien, E.O., Dietrich, D.R., 2009. Abundance and toxicity of *Planktothrix rubescens* in the pre-alpine Lake Ammersee, Germany. Harmful Algae 8, 329–342.

Fasham, M., Ducklow, H., Mckelvie, S., 1990. A nitrogen-based model of plankton dynamics in the oceanic mixed layer. J. Mar. Res. 48, 591–639.

Finkel, Z., Beardall, J., Flynn, K., Quigg, A., Rees, T., Raven, J., Raven, J.A., 2010. Phytoplankton in a changing world: cell size and elemental stoichiometry. J. Plankt. Res. 32, 119–137.

Flynn, K., Stoecker, D., Mitra, A., Raven, J., Glibert, P., Hansen, P.J., Graneli, E., Burkholder, J.M., 2012. Misuse of the phytoplankton-zooplankton dichotomy: the need to assign organisms as mixotrophs within plankton functional types. J. Plank. Res. 35, 3–11.

Flynn, K.J., Mitra, A., 2009. Building the "perfect beast": modelling mixotrophic plankton. J. Plank. Res. 31, 965–992.

Gal, G., Hipsey, M., Parparov, A., Wagner, U., Makler, V., Zohary, T., Zohary, T., 2009. Implementation of ecological modeling as an effective management and investigation tool: Lake Kinneret as a case study. Ecol. Model. 220, 1697–1718.
Gallina, N., Beniston, M., Jacquet, S., 2017. Estimating future cyanobacterial occurrence and importance in lakes: a case study with Planktothrix rubescens in Lake Geneva. Aquatic Sci. 79, 249–263.
Gentleman, W., Leising, A., Frost, B., Strom, S., Murray, J., 2003. Functional responses for zooplankton feeding on multiple resources: a review of assumptions and biological dynamics. Deep-Sea Res. II 50, 2847–2875.
Grover, J., 1991. Resource competition in a variable environment: phytoplankton growing according to the variable-internal-stores model. Am. Natural. 138, 811–835.
Grover, J., 2002. Stoichiometry, herbivory and competition for nutrients: simple models based on planktonic ecosystems. J. Theoret. Biol. 214, 599–618.
Halstvedt, C., Rohrlack, T., Andersen, T., Skulberg, O., Edvardsen, B., 2007. Seasonal dynamics and depth distribution of *Planktothrix spp*. in Lake Steinsfjorden (Norway) related to environmental factors. J. Plank. Res. 29, 471–482.
Hansen, P., Bjørnsen, P., Hansen, B., 1997. Zooplankton grazing and growth: Scaling within the 2–2,000-μm body size range. Limnol. Oceanogr. 42, 687–704.
Hessen, D.O., Elser, J.J., Sterner, R.W., Urabe, J., 2013. Ecological stoichiometry: an elementary approach using basic principles. Limnol. Oceanogr. 58, 2219–2236.
Hodge, S., Arthur, W., Mitchell, P., 1996. Effects of temporal priority on interspecific interactions and community development. Oikos 76, 350–358.
Hood, R.R., Laws, E.A., Armstrong, R.A., Bates, N.R., Brown, C.W., Carlson, C.A., Chai, F., Doney, S.C., Falkowski, P.G., Feely, R.A., Friedrichs, M.A.M., Landry, M.R., Moore, J.K., Nelson, D.M., Richardson, T.L., Salihoglu, B., Schartau, M., Toole, D.A., Wiggert, J.D., 2006. Pelagic functional group modeling: progress, challenges and prospects. Deep Sea Res. II 53, 459–512.
Jacquet, S., Briand, J.F., Christophe, L., Avois-Jacquet, C., Oberhaus, L., Tassin, B., Vinçon-Leite, B., Paolini, G., Druart, J.C., Anneville, O., Humbert, J.F., 2005. The proliferation of the toxic cyanobacterium *Planktothrix rubescens* following restoration of the largest natural French lake (Lac du Bourget). Harmful Algae 4, 651–672.
Jacquet, S., Domaizon, I., Anneville, O., 2014a. The need for ecological monitoring of freshwaters in a changing world: a case study of Lakes Annecy, Bourget, and Geneva. Environ. Monit. Assess. 186, 3455–3476.
Jacquet, S., Kerimoglu, O., Rimet, F., Paolini, G., Anneville, O., 2014b. Cyanobacterial bloom termination: the disappearance of *Planktothrix rubescens* from Lake Bourget (France) after restoration. Freshw. Biol. 59, 2472–2487.
Jöhnk, K., Huisman, J., Sharples, J., Sommeijer, B., Visser, P., Stroom, J., 2008. Summer heatwaves promote blooms of harmful cyanobacteria. Glob. Change Biol. 14, 495–512.
Jolliff, J., Kindle, J., Shulman, I., Penta, B., Friedrichs, M., Helber, R., Arnone, R., 2009. Summary diagrams for coupled hydrodynamic-ecosystem model skill assessment. J. Mar. Syst. 76, 64–82.
Kamjunke, N., Henrichs, T., Gaedke, U., 2007. Phosphorus gain by bacterivory promotes the mixotrophic flagellate Dinobryon spp. during re-oligotrophication. J. Plank. Res. 29, 39–46.
Kerimoglu, O., Straile, D., Peeters, F., 2012. Role of phytoplankton cell size on the competition for nutrients and light in incompletely mixed systems. J. Theor. Biol. 300, 330–343.
Kerimoglu, O., Straile, D., Peeters, F., 2013. Seasonal, inter-annual and long term variation in top-down versus bottom-up regulation of primary production. Oikos 122, 223–234.
Kiørboe, T., 2011. How zooplankton feed: mechanisms, traits and trade-offs. Biol. Rev. Camb. Philos. Soc. 86, 311–339.
Kondo, J., 1975. Air-sea bulk transfer coefficients in diabatic conditions. Bound. Layer Meteorol. 9, 91–112.
Konopka, A., 1982. Buoyancy regulation and vertical migration by *Oscillatoria Rubescens* in Crooked Lake, Indiana. Br. Phycolog. J., 427–442.
Kromkamp, J., Walsby, A.E., 1990. A computer model of buoyancy and vertical migration in cyanobacteria. J. Plankt. Res. 12, 161–183.
Kurmayer, R., Jüttner, F., 1999. Strategies for the co-existence of zooplankton with the toxic cyanobacterium *Planktothrix rubescens* in Lake Zürich. J. Plank. Res. 21, 659–683.
Le Vu, B., Vinçon-Leite, B., Lemaire, B., Bensoussan, N., Calzas, M., Drezen, C., Al, E., 2011. High-frequency monitoring of phytoplankton dynamics within the European water framework directive: application to metalimnetic cyanobacteria. Biogeochemistry 106, 229–242.
Litchman, E., Klausmeier, C.A., Schofield, O.M., Falkowski, P.G., 2007. The role of functional traits and trade-offs in structuring phytoplankton communities: scaling from cellular to ecosystem level. Ecol. Lett. 10, 1170–1181.
Litchman, E., Klausmeier, C.A., Yoshiyama, K., 2009. Contrasting size evolution in marine and freshwater diatoms. Proc. Natl. Acad. Sci. 106, 2665–2670.
Litchman, E., Pinto, P.D.T., Klausmeier, C.A., Thomas, M.K., Yoshiyama, K., 2010. Linking traits to species diversity and community structure in phytoplankton. Hydrolobiologia 653, 15–28.
Menden-Deuer, S., Lessard, E., 2000. Carbon to volume relationships for dinoflagellates, diatoms, and other protist plankton. Limnol. Oceanogr. 45, 569–579.
Mieleitner, J., Reichert, P., 2008. Modelling functional groups of phytoplankton in three lakes of different trophic state. Ecol. Model. 211, 279–291.
Mitra, A., Flynn, K.J., Burkholder, J.M., Berge, T., Calbet, A., Raven, J.a., Granéli, E., Glibert, P.M., Hansen, P.J., Stoecker, D.K., Thingstad, F., Tillmann, U., Våge, S., Wilken, S., Zubkov, M.V., 2014. The role of mixotrophic protists in the biological carbon pump. Biogeosciences 11, 995–1005.
Morel, F., 1987. Kinetics of nutrient uptake and growth in phytoplankton. J. Phycol. 23, 137–150.
Naselli-Flores, L., Barone, R., Chorus, I., Kurmayer, R., 2007. Toxic cyanobacterial blooms in reservoirs under a semiarid mediterranean climate: the magnification of a problem. Environ. Toxicol. 22, 399–404.
Oberhaus, L., Gelinas, M., Pinel-Alloul, B., Ghadouani, A., Humbert, J.F., 2007. Grazing of two toxic *Planktothrix* species by *Daphnia pulicaria*: potential for bloom control and transfer of microcystins. J. Plank. Res. 29, 827–838.
Omlin, M., Reichert, P., Forster, R., 2001. Biogeochemical model of Lake Zürich: model equations and results. Ecol. Model. 141, 77–103.
Oubelkheir, K., Sciandra, A., Babin, M., 2005. Bio-optical and biogeochemical properties of different trophic regimes in oceanic waters. Limnol. Oceanogr. 50, 1795–1809.
Padisák, J., Hajnal, É., Krienitz, L., Lakner, J., Üveges, V., 2010. Rarity, ecological memory, rate of floral change in phytoplankton and the mystery of the Red Cock. Hydrobiologia 653, 45–64.
Pahlow, M., Dietze, H., Oschlies, A., 2013. Optimality-based model of phytoplankton growth and diazotrophy. Mar. Ecol. Prog. Ser. 489, 1–16.
Paulson, C., Simpson, J., 1977. Irradience measurements in the upper ocean. J. Phys. Oceanogr. 7, 952–956.
Payne, R.E., 1972. Albedo of the Sea Surface. J. Atmos. Sci. 29, 959–970.
Posch, T., Salcher, M.M., Pernthaler, J., 2012. Harmful filamentous cyanobacteria favoured by reduced water turnover with lake warming. Nat. Clim. Change 2, 809–813.
Rinke, K., Yeates, P., Rothhaupt, K.O., 2010. A simulation study of the feedback of phytoplankton on thermal structure via light extinction. Freshw. Biol. 55, 1674–1693.
Robson, B.J., 2014. When do aquatic systems models provide useful predictions, what is changing, and what is next? Environ. Model. Softw. 61, 287–296.
Rosati, A., Miyakoda, K., 1988. A general circulation model for upper ocean simulation. J. Phys. Oceanogr. 18, 1601–1626.
Ryabov, A., Rudolf, L., Blasius, B., 2010. Vertical distribution and composition of phytoplankton under the influence of an upper mixed layer. J. Theor. Biol. 263, 120–133.
Salmaso, N., 2010. Long-term phytoplankton community changes in a deep subalpine lake: responses to nutrient availability and climatic fluctuations. Freshw. Biol. 55, 825–846.
Salmaso, N., Buzzi, F., Garibaldi, L., Morabito, G., Simona, M., 2012. Effects of nutrient availability and temperature on phytoplankton development: a case study from large lakes south of the Alps. Aquatic Sci. 74, 555–570.
Schwaderer, A., Yoshiyama, K., de Tezanos Pinto, P., Swenson, N.G., Klausmeier, C., Litchman, E., Litchman, E., 2011. Eco-evolutionary differences in light utilization traits and distributions of freshwater phytoplankton. Limnol. Oceanogr. 56, 589–598.
Shimoda, Y., Arhonditsis, G., 2016. Phytoplankton functional type modelling: Running before we can walk? A critical evaluation of the current state of knowledge. Ecol. Model. 320, 29–43.
Sommer, U., Adrian, R., Domis, L.D.S., Elser, J.J., Gaedke, U., Ibelings, B., Jeppesen, E., Lürling, M., Molinero, J.C., Mooij, W.M., Donk, E.V., Winder, M., 2012. Beyond the Plankton Ecology Group (PEG) Model: mechanisms driving plankton succession. Annu. Rev. Ecol. Evol. Syst. 43, 429–448.
Sommer, U., Lewandowska, A., 2011. Climate change and the phytoplankton spring bloom: Warming and overwintering zooplankton have similar effects on phytoplankton. Glob. Change Biol. 17, 154–162.
Steele, J., Henderson, E., 1992. The role of predation in plankton models. J. Plank. Res. 14, 157–172.
Straile, D., 1997. Gross growth efficiencies of protozoan and metazoan zooplankton and their dependence on food concentration, predator-prey weight ratio, and taxonomic group. Limnol. Oceanogr. 42, 1375–1385.
Tapolczai, K., Anneville, O., Padisák, J., Salmaso, N., Morabito, G., Zohary, T., Tadonléké, R., Rimet, F., 2014. Occurrence and mass development of *Mougeotia* spp. (Zygnemataceae) in large, deep lakes. Hydrobiologia 745, 17–29.
Terseleer, N., Bruggeman, J., Lancelot, C., Gypens, N., 2014. Trait-based representation of diatom functional diversity in a plankton functional type model of the eutrophied southern North Sea. Limnol. Oceanogr. 59, 1958–1972.
Thingstad, T., Havskum, H., Garde, K., Riemann, B., 1997. On the strategy of 'eating your competitor': a mathematical analysis of algal mixotrophy. Ecology 77, 2108–2118.
Vinçon-Leite, B., Lemaire, B.J., Khac, V.T., Tassin, B., 2014. Long-term temperature evolution in a deep sub-alpine lake, Lake Bourget, France: how a one-dimensional model improves its trend assessment. Hydrobiologia 731, 49–64.
Vinçon-Leite, B., Tassin, B., Druart, J.C., 2002. Phytoplankton variability in Lake Bourget: phytoplankton dynamics and meteorology. Lakes Reserv. 7, 93–102.
Vinçon-Leite, B., Tassin, B., Jaquet, J.M., 1995. Contribution of mathematical modeling to lake ecosystem understanding: Lake Bourget (Savoy, France). Hydrobiologia 300/301, 433–442.
Walsby, A., Avery, A., Schanz, F., 1998. The critical pressures of gas vesicles in *Planktothrix rubescens* in relation to the depth of winter mixing in Lake Zurich, Switzerland. J. Plank. Res. 20, 1357–1375.
Walsby, A.E., Ng, G., Dunn, C., Davis, P.A., 2004. Comparison of the depth where *Planktothrix rubescens* stratifies and the depth where the daily insolation supports its neutral buoyancy. New Phytolog. 162, 133–145.
Walsby, A.E., Schanz, F., 2002. Light-dependent growth rate determines changes in the population of *Planktothrix rubescens* over the annual cycle in Lake Zürich, Switzerland. New Phytolog. 154, 671–687.

Ward, B., Dutkiewicz, S., Jahn, O., Follows, M.J., 2012. A size-structured food-web model for the global ocean. Limnol. Oceanogr. 57, 1877–1891.
Ward, B.A., Follows, M.J., 2016. Marine mixotrophy increases trophic transfer efficiency, mean organism size, and vertical carbon flux. Proc. Natl. Acad. Sci. 113, 2958–2963.
Wirtz, K., Kerimoglu, O., 2016. Optimality and variable co-limitation controls autotrophic stoichiometry. Front. Ecol. Evol.
Wirtz, K.W., 2013. Mechanistic origins of variability in phytoplankton dynamics: Part I: niche formation revealed by a size-based model. Mar. Biol. 160, 2319–2335.